

# In-circuit RF impedance measurement for EMI filter design in switched mode power supplies

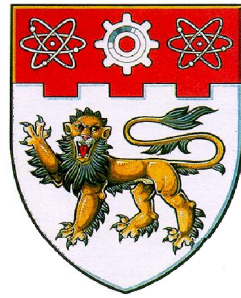
Deng, Junhong

2008

Deng, J. (2008). In-circuit RF impedance measurement for EMI filter design in switched mode power supplies. Doctoral thesis, Nanyang Technological University, Singapore.

<https://hdl.handle.net/10356/14565>

<https://doi.org/10.32657/10356/14565>



**NANYANG  
TECHNOLOGICAL  
UNIVERSITY**

**IN-CIRCUIT RF IMPEDANCE MEASUREMENT FOR  
EMI FILTER DESIGN IN SWITCHED MODE POWER  
SUPPLIES**

IN-CIRCUIT RF IMPEDANCE MEASUREMENT FOR EMI FILTER  
DESIGN IN SWITCHED MODE POWER SUPPLIES

DENG JUNHONG

DENG JUNHONG

SCHOOL OF ELECTRICAL AND ELECTRONIC  
ENGINEERING

2008

2008

# **IN-CIRCUIT RF IMPEDANCE MEASUREMENT FOR EMI FILTER DESIGN IN SWITCHED MODE POWER SUPPLIES**

DENG JUNHONG

School of Electrical and Electronic Engineering

A thesis submitted to the Nanyang Technological University  
in fulfillment of the requirement for the degree of  
Doctor of Philosophy

2008


## **Statement of Originality**

I hereby certify that the content of this thesis is the result of work done by me and has not been submitted for a higher degree to any other University or Institution.

3 Sept 2008

---

Date



---

Deng Junhong

## **Acknowledgements**

The work presented in this thesis has been carried out under the supervision of Dr. See Kye Yak, Associate Professor, School of Electrical and Electronic Engineering, Nanyang Technological University. I would like to express my most sincere gratitude to him for his guidance and support throughout this research.

I also would like to express my deepest gratitude to my wife and my daughter for their understanding and support throughout the course of this research project.

## Summary

To design an electromagnetic interference (EMI) suppression filter for a switched mode power supply (SMPS) systematically, information of the noise source impedance and noise terminating load impedance is essential for selecting the most appropriate filter configuration and choosing the respective filter elements' values. Based on a two-current-probe measurement approach, a novel method to determine both common-mode (CM) and differential-mode (DM) noise source impedance of an SMPS has been developed. The proposed method allows measurement of noise source impedance of an SMPS under its normal powered on condition. With proper pre-measurement calibration, it is capable of deriving noise source impedance of SMPS in terms of equivalent electrical circuit model with good accuracy. Once the equivalent electrical model of the noise source impedance is derived through measurement, the most effective filter configuration and component's value for the built-in EMI filter of the SMPS could be designed without the usual guessing approach.

The effectiveness of power line EMI filter in the SMPS depends to a great extent on the characteristics of the filter components under actual loading conditions, especially the common-mode (CM) EMI suppression chokes. However, the CM choke's parameters given by the manufactures are usually measured under no load or direct current (dc) loading condition, from which the information of core saturation and parasitic effects under the actual operating condition are not fully reflected. With a

novel measurement setup, the two-current-probe method is further extended to measure the CM and DM suppression characteristics of the CM choke, as well as the DM suppression characteristic of DM choke, under in-circuit operating condition. The proposed in-circuit measurement approach provides a more realistic assessment of the EMI suppression of any EMI suppression choke with good confidence.

# Contents

Acknowledgements .....	i
Summary .....	ii
List of Figures .....	vi
List of Tables.....	ix
List of Abbreviations .....	x
Chapter 1 Introduction.....	1
1.1 Background.....	1
1.2 Motivation.....	3
1.3. Literature Review .....	5
1.4 Objective.....	15
1.5 Thesis Organization.....	15
Chapter 2 Conducted Emissions and EMI Filters in SMPS.....	17
2.1 Conducted Emissions .....	17
2.2 Power Line EMI Filters .....	24
2.3 EMI Filter Design .....	30
2.4 Insertion Loss Measurement.....	41
Chapter 3 Two-Current-Probe Method.....	49
3.1 Introduction.....	49
3.2 Theoretical Background .....	51
3.3 Measurement Setup with a Spectrum Analyzer and a Signal Generator..	56



3.5	Validation .....	61
Chapter 4	Measurement of Noise Source Impedance of SMPS.....	68
4.1	Noise Source Impedance of SMPS .....	68
4.2	Measurement with the two Current Probes Method.....	72
4.3	Experiment Results .....	76
Chapter 5	Characterization of EMI Chokes .....	83
5.1	EMI Filter Components .....	83
5.2	EMI Chokes .....	86
5.3	In-Circuit Characterization of EMI Chokes .....	94
5.4	Experiment Results .....	100
Chapter 6	Conclusions .....	107
References	.....	109
Publications by the Author	.....	118

## List of Figures

Figure 1.1	Test setup of the resonance method.....	7
Figure 1.2	Simplified noise emissions model in insertion loss method .....	11
Figure 1.3	Series insertion method.....	12
Figure 1.4	Shunt insertion method .....	12
Figure 2.1	The circuit diagram of a $50\ \Omega / 50\ \mu\text{H}$ LISN .....	21
Figure 2.2	Impedance-frequency characteristic of the $50\Omega/50\mu\text{H}$ LISN .....	22
Figure 2.3	CM and DM noise currents in conducted emissions measurement .....	22
Figure 2.4	load voltage without the filter - definition of the insertion loss.....	26
Figure 2.5	load voltage with the filter - definition of the insertion loss of a filter ....	26
Figure 2.6	CM equivalent circuit without any filter components .....	32
Figure 2.7	CM equivalent circuit with 2 <sup>nd</sup> order CM filter.....	32
Figure 2.8	CM equivalent circuit with 3 <sup>rd</sup> order CM filter .....	33
Figure 2.9	$\pi$ Filter .....	39
Figure 2.10	Typical EMI filter circuit of switched mode power supply .....	40
Figure 2.11	No-load $50\Omega$ CM insertion loss measurement .....	42
Figure 2.12	No-load $50\Omega$ DM insertion loss measurement .....	43
Figure 2.13	Basic test circuit for insertion loss measurement with full load .....	44
Figure 2.14	Series injection worst case insertion loss measurement system .....	48
Figure 2.15	Parallel injection worst case insertion loss measurement system .....	48

Figure 3.1	Basic setup of the two-current-probe method with network analyzer .....	52
Figure 3.2	The equivalent circuit of the two-current-probe measurement setup .....	52
Figure 3.3	Simplified equivalent circuit of the two-current-probe setup .....	53
Figure 3.4	Measurement setup with a spectrum analyzer and a signal generator ....	58
Figure 3.5	Setup using a spectrum analyzer with an internal tracking generator ....	59
Figure 3.6	Induced signal and background RF noise .....	60
Figure 3.7	Measurement setup in validation .....	63
Figure 3.8	Measurement of large-resistance resistors .....	64
Figure 3.10	Comparison of measured results for $5\ \Omega$ .....	65
Figure 3.11	Comparison of measured results for $5\ \text{k}\Omega$ .....	65
Figure 3.12	Comparison of results obtained with SA and VNA .....	67
Figure 4.1	CM source impedance of SMPS .....	69
Figure 4.2	DM source impedance of SMPS .....	70
Figure 4.3	Simplified noise source circuit.....	70
Figure 4.4	Measurement setup of SMPS's CM noise source impedance .....	74
Figure 4.5	Measurement setup of SMPS's DM noise source impedance .....	75
Figure 4.6	Implementation of the RF coupling circuit.....	77
Figure 4.7	CM noise source impedance measurement.....	80
Figure 4.8	DM noise source impedance measurement .....	81
Figure 4.9	Comparison of the measured and calculated $Z_{\text{setup}}$ .....	82
Figure 4.10	Comparison of the measured and calculated $Z_T$ .....	82

Figure 5.1	Structure of CM EMI choke.....	87
Figure 5.2	Structure of DM single-layer solenoid choke.....	90
Figure 5.3	Equivalent circuit of an EMI choke .....	91
Figure 5.4	Impedance versus frequency of an EMI choke .....	93
Figure 5.5	Measurement setup to characterize CM impedance of a CM choke .....	96
Figure 5.6	Measurement setup to characterize DM impedance of a CM choke .....	98
Figure 5.7	Measurement setup to characterize DM choke.....	99
Figure 5.8	Measurement setup for characterization of chokes in laboratory.....	102
Figure 5.9	Circuit built in laboratory for the measurement of CM choke .....	103
Figure 5.10	The CM impedance and $Z_{\text{setup}}$ .....	104
Figure 5.11	The measured CM impedance of the CM choke .....	104
Figure 5.12	Circuit for the measurement of CM choke's DM impedance .....	106
Figure 5.13	The measured DM impedance of the CM choke .....	106

## List of Tables

Table 1	The first and second order filter selection matrix .....	29
Table 2	The higher order filter selection matrix .....	29
Table 3	Maximum leakage current defined in IEC 60950-1: 2005.....	36

## List of Abbreviations

AMN	Artificial Mains Network
ANSI	American National Standards Institute
CISPR	Comite International Special des Perturbations Radioelectriques
CM	Common Mode
DM	Differential Mode
FET	Field-Effect Transistor
EM	Electromagnetic
EMC	Electromagnetic Compatibility
EMI	Electromagnetic Interference
ESD	Electrostatic Discharge
ESL	Equivalent Series Inductance
ESR	Equivalent Series Resistance
EUT	Equipment Under Test
IC	Integrated Circuit
IEC	International Electrotechnical Commission
IGBT	Insulated Gate Bipolar Transistor
LISN	Line Impedance Stabilization Network
MOSFET	Metallic Oxide Semiconductor Field Effect Transistor
PCB	Printed Circuit Board
RF	Radio Frequency
SMPS	Switched Mode Power Supply

# Chapter 1 Introduction

## 1.1 Background

Many well-established filter design methodologies for addressing and solving electromagnetic compatibility (EMC) problems in telecommunications have been developed over the years. Unfortunately, these methods cannot be applied directly to the field of power electronics. Design equations for low pass EMI filters used in RF and microwave applications are not applicable to SMPS. These equations were developed for well defined matched source and load impedances, for example,  $50\Omega$ . Such conditions do not exist in power electronic circuits. Also, the EMI filter is connected directly to high voltage power lines and is designed for much higher current rating. Another constraint for designing power line EMI filter is the restrictions in values for both the serial and the parallel filter elements. For examples, the value of the serial inductance is limited by maximum allowable voltage drop at the operating frequency and the value of line-to-ground capacitor (parallel element) is limited by the acceptable ground leakage current for safety purposes.

Conducted emissions produced by SMPS are usually broadband and coherent. They appear in the form of common-mode (asymmetrical) and differential-mode (symmetrical) currents. The noise source impedance of an SMPS varies widely, as it

depends on the circuit configuration, the layout technology and the semiconductor switch. To make the EMI filter design more complicated, the noise source impedance is also frequency-dependent. Moreover, the semiconductor switches in the SMPS are switching at high frequency in SMPS's normal operation, which makes the impedance analysis even more challenging.

Unlike filters in RF and microwave circuits, EMI suppression filters in SMPS are terminated with varying source and load impedances. In addition, the power handling requirements of the filter elements decide many of the filter parameters, such as saturation current, leakage inductance, breakdown voltage, wire size and core size. Information of the source and load impedances is vital for selecting the most effective filter configuration and filter components for SMPS.

The effectiveness of power line EMI filter in the SMPS depends to a great extent on the characteristics of the power line filter components under the actual operating condition. However, the specifications of filter components supplied by manufactures are mostly obtained from 50  $\Omega$  measurement system under no load condition. For examples, the specifications of EMI suppression inductors usually do not indicate information of core saturation effects. Therefore, the ability to extract the characteristics of the power line filter elements such as common-mode (CM) and differential-mode (DM) chokes under actual operating condition is also an important aspect of power line EMI filter design.



## 1.2 Motivation

The motivation of the research work presented in this thesis aims to establish a systematic power line EMI filter design methodology. To facilitate this systematic design methodology, the information on the noise source impedance and filter components' characteristics under actual operating condition is important.

### 1.2.1 Noise Source Impedance of Switched Mode Power Converter

Optimal power line filter configuration as well as filter component values can be properly chosen [1][2][3], without the usual trial-and-error process, if the source and load impedances are known. With the known source and load impedances, the filter design process can be done efficiently to meet EMI requirements.

The international EMI measurement standards specify a line impedance stabilization network (LISN) be used in the conducted emissions measurement. The LISN provides stable well-defined power mains impedance for the purpose of measurement repeatability [4][5][6][7]. By supplying AC power to SMPS-under-test through the LISN, the terminating impedance of the noise source (the SMPS) is properly defined. However, the equivalent noise source impedance of the SMPS, is not readily available [8]. Thus the development of a method that allows accurate and

reliable measurement of noise source impedance of a SMPS will be able to provide this useful information.

The CM noise source impedance is found to be dominated by the unintentional capacitance between the switching device and the ground. The unintentional capacitance can be contributed by parasitic capacitance between the heat sink and the grounded chassis, and parasitic capacitance between other devices or wires and the grounded chassis. The major contributors of DM noise source impedance are the turned-on resistance of rectifying diodes, and the equivalent series resistance (ESR) and equivalent series inductance (ESL) of the DC filtering capacitor. Other factors, such as the PCB layout, component placement and wiring layout also influence the noise source impedance. Due to the complexity of the CM and DM noise coupling mechanisms, complete theoretical models may not be easily derived [10]. Hence, the best way to determine their characteristics is still through measurement.

### **1.2.2 RF Impedance of EMI Suppression Chokes**

Two supposedly identical power line filter elements from two different manufacturers may perform differently in the same design application. In the case of filter chokes, no information about the operating current at which the inductors, both common core and independent core, will saturate, has been given. Hence, two supposedly identical filter chokes may perform very differently, depending of the core material used.

Various measurement methods have been developed to measure the EMI suppression chokes under either steady-state DC or AC load current with defined source and load impedances [11] . In reality, for EMI filters in power conversion applications, the current carried by the chokes is usually a pulsed DC current under varying source impedance [14]. The characteristics of an EMI suppression choke under realistic operating condition may not be easily determined with existing methods or through theoretical analysis due to the complexity of the actual operating condition. The development of a measurement method to characterize the chokes under realistic operating condition will be useful.

### **1.3. Literature Review**

#### **1.3.1 Noise Source Impedance of Switched Mode Power Converter**

##### **1.3.1.1 Resonance Method**

Schneider [16] proposed a resonance method to estimate the noise source impedance of a SMPS by terminating the power input of the SMPS with a reactive component that is opposite type to the noise source reactance. In this method, the noise source of a SMPS is treated as a black box, which is represented as a Norton equivalent circuit with a constant current source and a reactance. By careful choice of the terminating load impedance for the noise source, the Norton equivalent circuit of

the noise source can be estimated. The value of the constant current source is obtained by terminating the noise source with a short circuit. By selecting a reactive load that resonates with the source's reactive impedance, we can obtain the  $Q$  factor of the parallel resonant circuit at a specific frequency. The  $Q$  factor of the circuit is defined as:

$$Q = \frac{I_l}{I_0} \quad (1-1)$$

where  $I_l$  is the measured current under resonant condition and  $I_0$  is the measured current under short circuit condition.

The concept of the resonance method is illustrated by the test setup shown in Figure 1.1, where the Norton equivalent circuit of the noise source is assumed to be a constant current source with resistive source resistance  $R$  and capacitive source capacitance  $C$  in parallel (CM case). A current probe is inserted between the noise source and terminating inductive load  $L$ , which measures the current in the test setup. When the switch is in closed position, the current measured is equal to  $I_0$ , which is the magnitude of the constant current source. When the switch is in opened position, the terminating load inductor is tuned to resonate with the noise source capacitive reactance, and the resonant current  $I_l$  circulating between  $L$  and  $C$  is measured.

Under the resonant condition,

$$RI_0 = \omega LI_l \quad (1-2)$$

$$RI_0 = \frac{I_l}{\omega C} \quad (1-3)$$

Substituting equation 1-1 into equations 1-2 and 1-3,

$$Q = \frac{I_l}{I_0} = \frac{R}{\omega L} \quad (1-4)$$

$$Q = \frac{I_l}{I_0} = \omega CR \quad (1-5)$$

Hence, the  $Q$  can be used to determine the resistive and reactive components of the noise source impedance.

Similarly, we are also able to make the measurement with the resonant method for the noise source with a Norton equivalent circuit which consists of a constant current source, a resistive source resistance  $R$  and a inductive source inductor  $L$  in parallel (DM case).

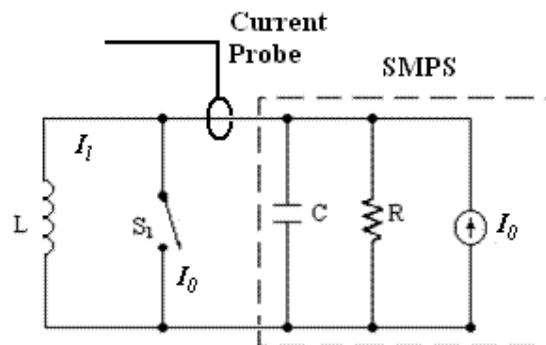


Figure 1.1 Test setup of the resonance method

Theoretically, the resonance method looks rather simple. In practice, the process to choose the right values of reactive components and to tune for resonance can be very tedious and cumbersome. All reactive components are non-ideal in nature and the calculation given in this method only provides rough estimation of the noise source impedance. Especially when the frequency of measurement is high, the parasitic effects of those non-ideal reactive components become significant and the circuit topology based on which the resonance method is developed is no longer valid. For the reason just mentioned, the resonance method is only valid if conducted properly below 1 MHz. For the case of the CM noise source impedance measurement, the range of value can be measured depends very much on the adjustable range of the inductor. Selecting the right inductor with sufficient tuning range to achieve the required resonant at a predetermined frequency may not always be possible practically. For the case of the DM noise source impedance measurement, attempts to achieve resonant are very difficult because of the low-impedance nature of the DM noise source. The calculation given in this method only provides rough estimate of the noise source impedance.

### **1.3.1.2 The insertion loss method**

Another method, the insertion loss method [17], has also been introduced to measure the noise source impedance of an SMPS. In the insertion loss method, the noise source of a SMPS is simplified to a one-port Thevenin equivalent circuit shown in Figure 1.2, where  $Z_s$  can be referred to as either CM or DM noise source impedance.

To obtain  $Z_s$  through measurement, a filter element, either a series element  $Z_{series}$  or a shunt element  $Z_{shunt}$ , is inserted between noise source and noise load (a LISN in actual measurement) shown in Figure 1.3 and Figure 1.4. With the filter element inserted, the noise voltage across the load  $R_{load}$  changes, and the amount of change is measured in terms of the insertion loss A. The insertion loss A is defined as the ratio of voltage across  $R_{load}$  before and after the filter element is inserted. From the measured insertion loss and the known impedance of the inserted filter element, the magnitude of noise source impedance  $|Z_s|$  can be calculated. To obtain  $|Z_s|$  with good accuracy, either series insertion method or shunt insertion method is used, depending on the relative magnitude of  $|Z_s|$  versus  $R_{load}$ .

In the case of  $|Z_s| \gg R_{load}$ , the series insertion method is used for better accuracy. Based on the assumption  $|Z_{series}| \gg |Z_s|$ , the expression for insertion loss A can be simplified as follows:

$$A = \frac{\frac{R_{load}}{R_{load} + Z_s} \times V_s}{\frac{R_{load}}{R_{load} + Z_s + Z_{series}} \times V_s} = 1 + \frac{Z_{series}}{R_{load} + Z_s} \approx 1 + \frac{Z_{series}}{Z_s} \quad (1-6)$$

Since the insertion loss is normally much greater than 1, equation 1-6 can be approximate by:

$$|Z_s| \approx \frac{|Z_{series}|}{|A|} \quad (1-7)$$

Where  $|Z_{series}|$  is given and  $|A|$  can be obtained by the insertion loss measurement,  $|Z_s|$  can be calculated with 1-7. Generally speaking, the larger the insertion loss is, the more accurate the equation 1-7 is.

In the case of  $|Z_s| \ll R_{load}$ , the shunt insertion method is used for better accuracy. Based on the assumption  $|Z_{shunt}| \ll |Z_s|$ , the expression for insertion loss A can be simplified as follows:

$$A = \frac{\frac{R_{load}}{R_{load} + Z_s} \times V_s(\omega)}{\frac{R_{load} // Z_{shunt}}{R_{load} // Z_{shunt} + Z_s} \times V_s(\omega)} = 1 + \frac{R_{load} // Z_s}{Z_{shunt}} \approx 1 + \frac{Z_s}{Z_{shunt}} \quad (1-8)$$

Similarly, the insertion loss is normally much greater than 1, equation 1-8 can be approximate by:

$$|Z_s| \approx |Z_{shunt}| \times |A| \quad (1-9)$$

Where  $|Z_{shunt}|$  is given and  $|A|$  can be obtained by the insertion loss measurement,  $|Z_s|$  can be calculated with equation 1-9.

In the case of  $|Z_s|$  and  $R_{load}$  are of comparable magnitude:  $R_{load}$  can be decreased or increased so that either  $|Z_s| \gg R_{load}$  or  $|Z_s| \ll R_{load}$  is satisfied.

The first step of the measurement is to decide which insertion loss method to be used without first knowing the magnitude of  $|Z_s|$ . We can start with the series insertion method first. From equation 1-6,  $|R_{load} + Z_s|$  can be found. If the value of



$|R_{load} + Z_s|$  turns out to be much greater than  $R_{load}$ , then the condition  $|Z_s| \gg R_{load}$  is valid. Similarly, we can also try the shunt insertion method and determine  $|R_{load} // Z_s|$  using equation 1-8. If  $|R_{load} // Z_s|$  is much smaller than  $R_{load}$ , then the condition  $|Z_s| \ll R_{load}$  is satisfied.

$Z_s$  is a complex function of frequency in general. The magnitude of  $Z_s$  can be found easily by either equation 1-7 or equation 1-9. However, the phase of  $Z_s$  cannot be found from the same equations. In many applications, the phase of  $Z_s$  is inconsequential. In cases the phase is desired, Hilbert transform can be used to derive it. Hilbert transform basically establishes a relationship between the phase  $\angle Z_s(\omega)$  and magnitude  $|Z_s(\omega)|$  of a minimum phase function such as the impedance function [17]:

$$\angle Z_s(\omega) = \frac{2\omega}{\pi} \int_0^\infty \frac{|Z_s(\xi)| - |Z_s(\omega)|}{(\xi + \omega)(\xi - \omega)} d\xi \quad (1-10)$$

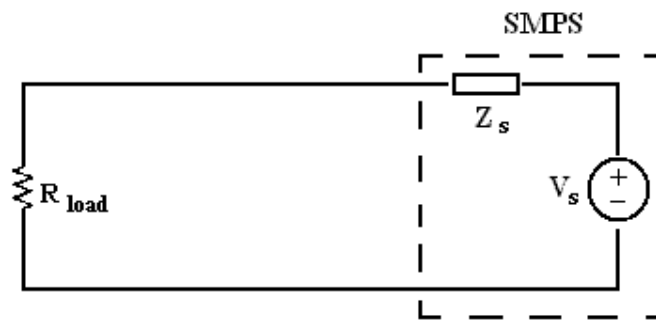


Figure 1.2 Simplified noise emissions model in insertion loss method

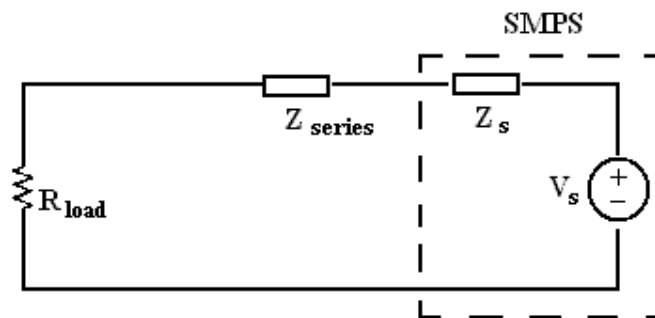


Figure 1.3 Series insertion method

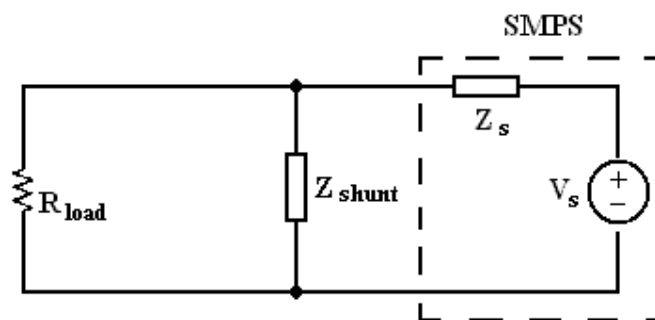


Figure 1.4 Shunt insertion method

As long as the magnitude function  $|Z_s(\omega)|$  is known over a fairly wide frequency range, for example  $0 \sim f_{\max}$ , the phase function  $\angle Z_s(\omega)$  can usually be found quite accurately at least up to  $f_{\max}/3$ . In most practical situations, the model of noise source impedance is simple. The variation of the magnitude of the impedance with increasing frequency will provide enough information of the characteristics of the impedance. For

example, if the noise source impedance is capacitive in nature, the magnitude of its impedance with increasing frequency will show a decreasing trend of -20 dB/decade.

Similar to the resonance method, the insertion loss method also looks simple. However, the condition for the impedance of the inserted filter element to be either much larger or smaller than the noise source impedance may not always be feasible. The parasitic effects of those non-ideal filter elements make the condition even more difficult to be fulfilled. Also, in reality, a CM or DM filter element does not only affect its own conduction mode but also the other mode. For example, in the CM insertion loss measurement, there is leakage inductance in the CM choke and it affects the DM noise as well. Therefore, the CM insertion loss measured is not due only to CM alone. Hence, accuracy deteriorates if the conditions required in this method are not met.

### **1.3.2 RF Impedance of EMI Suppression Chokes**

Inductance value measurements are normally made at very low values of voltage, current, and frequency using a bridge instrument or a LCR meter. In recent years, current biased LCR meters also are available in the market. The usual measurement frequency is 1kHz. The self-resonant frequency which is due to the capacitance within the coil winding, the distributed capacitance, is not found in the low-frequency measurements. For EMI filter application, the frequency range over which the inductor's performance is evaluated is up to and above 30MHz. The traditional low

frequency method with this type of instrument is not suitable to evaluate the EMI chokes.

Traditionally, filter components are normally evaluated under no load condition by means of a 50  $\Omega$  measurement system with RF impedance analyzer, network analyzer or some special measurement setup. Hence, the impedance characteristics of the filter components provided by the manufacturers in the product specifications are based on the 50  $\Omega$  measurement system at no load condition. This may be true for RF/microwave design applications but in power electronics applications, the power line EMI filter components are operating at very high voltage as well as high current loading condition. For filter chokes, saturation and core loss of the magnetic core materials are rather sensitive to the loading condition. Also, actual impedance where the power line EMI filter chokes to be inserted is not 50 $\Omega$ .

The another approach is using insertion loss method to characterize the EMI chokes by treating the choke as a one element EMI filter. The test methods described in the standards ANSI C63.13 [11], CISPR 17 [12] and MIL-STD-220B [13] can be used to perform the insertion loss measurement for the one element EMI filter under various loading conditions such as no-load, steady-state DC or AC load current with various defined source and load impedances. However, all these methods do not characterize the chokes under their actual operating configuration. For EMI filters in power conversion applications, the current carried by the EMI choke is usually a pulsed DC, which is significantly different from the loading condition specified in the standards. In addition, the noise source impedance of the SMPS can vary widely, which can be significantly different from the impedance used in the standards. Hence,

the EMI suppression performance of the EMI choke cannot be evaluated correctly with the methods.

## **1.4 Objective**

In order to design a power line filter for a SMPS systematically, the characteristics of CM and DM noise impedances over the frequency range of interest, for example, 150 kHz-30 MHz in most conducted emissions regulations, must be known. In addition, the effectiveness of an EMI suppression choke depends to a great extent on its impedance characteristics under a specific current loading condition.

The objective of the thesis is to develop a suitable measurement method so that it is able to characterize CM and DM noise source impedances of SMPS as well as EMI suppression choke under actual operating condition in the frequency range of 150 kHz – 30MHz.

## **1.5 Thesis Organization**

The thesis is organized into six chapters.

Chapter 1 gives an overview of the thesis. Literature review, motivation and objective are described.

Chapter 2 provides the necessary fundamentals covering conducted emission measurement, discrimination of common-mode (CM) and differential-mode (DM) conducted emissions, mechanism of conducted emissions in the SMPS, EMI filter configurations, EMI filter design, EMI filter components and insertion loss measurement.

In Chapter 3, the basic theory of a two-current-probe method is presented. Two measurement approaches have been discussed. The first approach is two-probe measurement with a network analyzer. The second approach is two-probe measurement with a spectrum analyzer and a signal generator to improve the signal-to-noise performance. After comparison of the two approaches, the second approach is chosen. The validation of proposed measurement method is also provided in this chapter.

Based on the two-current-probe measurement method, characterization of CM and DM noise source impedances of SMPS is explained in Chapter 4. This characterization approach allows measurement of noise source impedance of the SMPS without interrupting its normal operation. The proposed measurement method is demonstrated with an actual measurement on an SMPS.

In Chapter 5, the two-current-probe method is extended to characterize the impedance of EMI chokes, with a modified test setup. The proposed measurement method provides a more realistic assessment of the impedance characteristic of EMI chokes under actual operating condition with good accuracy.

Finally, Chapter 6 concludes the thesis and discusses future work that is worth exploring.

## **Chapter 2      Conducted Emissions and EMI Filters in Switched Mode Power Supplies**

### **2.1      Conducted Emissions**

#### **2.1.1      Electromagnetic Compatibility**

Electromagnetic compatibility (EMC) is the ability of an equipment or system to function satisfactorily in its electromagnetic environment without introducing intolerable electromagnetic disturbances to anything in that environment [18]. In essence, the definition of EMC emphasizes two aspects, emission and immunity. Emission is the phenomenon by which electromagnetic energy emanates from a source. Immunity is the ability of a device, equipment or system to perform without degradation in the presence of an electromagnetic disturbance.

Electromagnetic Interference (EMI) is defined as a phenomenon where an electronic device or system generates electromagnetic (EM) field in the radio-frequency (RF) spectrum that degrades the satisfactory operation of other electronic device or system in its vicinity. EMC is achieved when a piece of electronic

## ***Chapter 2 Conducted Emissions and EMI Filters in Switch Mode Power Supplies***

---

equipment functions satisfactorily in its intended electromagnetic environment and does not introduce intolerable EMI to affect anything in that environment.

The evolution of technology has caused EMC design to be as critical a part of electronic design as any of the traditional aspects. The primary concern of EMC engineering design is to make electronic systems to comply with the legal requirements imposed by governmental agencies. These EMC regulations have made EMC a critical aspect in the marketability of an electronic product. If the product does not comply with these regulations for a particular country, it cannot be sold in that country. The primary advantages of adequate EMC design consideration at the early design stage are:

1. Minimizing the needs of redesigning in order to satisfy the EMC regulatory requirements and hence, eliminating additional product development cost.
2. Maintaining the product launch schedule and avoiding delay in penetrating the market.
3. Ensuring the product operates satisfactorily in the presence of the inevitable external noise sources at its installation location, and hence minimizing customer complaints.

The best practice in ensuring the product satisfying the EMC regulatory requirements with minimum costs is to consider EMC design in the early stage of the product development cycle.



### **2.1.2 Conducted Emissions Measurement**

Electromagnetic emissions occur not only by electromagnetic waves propagating through air but also by direct conduction on metallic conductors. Usually, for typical electronic products, emissions by conduction are more efficient than air coupling path at the lower frequency range. Hence, conducted emissions measurement defined in EMC standards is usually covered from 150k Hz to 30 MHz in most international standards. For emissions higher than 30 MHz, they are more efficient to propagate through radiation in air. Noise current conducted out the ac cord passes through the commercial power distribution net of the installation. This commercial power distribution net is an extensive array of wires connecting the various power outlets from which the other electronic systems in the installation receive their ac power. It therefore represents a large "antenna" system from which these conducted emissions can radiate quite efficiently, causing interference in the other electronic systems of the installation. Therefore, controlling conducted emissions of a product indirectly also controls the radiated emissions [19].

The purpose of the conducted emissions test is to measure the noise current that exits the product's ac power cord. These emissions could be simply measured with a current probe. However, for measurement repeatability, between sites, this simple measurement method is not good enough. The impedance looking into the ac mains power outlet varies considerably over the measurement frequency range from outlet to outlet and building to building [20]. Such impedance variation affects the amount of

## ***Chapter 2 Conducted Emissions and EMI Filters in Switch Mode Power Supplies***

---

noise that is conducted out the power cord. To ensure consistency of measurement results between test sites, the ac mains impedance seen by the product must be well-defined and stable regardless of the measurement site.

To overcome the problem of measurement repeatability, the line impedance stabilization network (LISN) has been developed and designed for conducted emission measurement. Its primary objective is to present constant ac mains impedance to the product under test over the frequency range of the conducted emission test. Its other objective is to block conducted emissions from the ac mains that are not due to the product under test so that only the conducted emissions of the product are measured.

Besides these two objectives, the LISN also provides easy interface to the measuring receiver without direct contact to the high voltage ac mains. Figure 2.1 shows the schematic circuit of a typical LISN.

The impedance at the disturbance output terminal (the terminal connected to the EMI measuring receiver) of the LISN defines the termination impedance presented to the equipment-under-test (EUT). For this reason, when a disturbance output terminal is not connected to the measuring receiver, it shall be terminated by a 50  $\Omega$  dummy termination. Figure 2.2 shows the impedance versus frequency of the LISN defined in the CISPR 16-1 standard.

Conducted emissions appearing on the live and neutral wires of the EUT may be resolved into two conduction modes, differential-mode (DM) and common-mode (CM). DM current flows in live wire in one direction and returns in the opposite direction in neutral wire. CM current flows in the same direction in both wires and returns via the earth wire. Figure 2.3 shows the two noise conduction modes in a

## Chapter 2 Conducted Emissions and EMI Filters in Switch Mode Power Supplies

conducted emission measurement setup. An understanding of the two conduction modes will facilitate the systematic design of an EMI filter.

The ability to discriminate DM and CM conducted emissions is essential for conducted EMI diagnosis and power line EMI filter design. In the conducted emission compliance test, the emission measured with the LISN is a mixture of both DM and CM noise. When the conducted noise fails to satisfy the limits specified in the EMC standards, it is usually not easy to identify the dominant mode that causes the failure. Furthermore, power line EMI filter design is also divided into CM and DM filters, which make the discrimination of the noise be essential in filter design process. Many different CM and DM conducted emission discrimination techniques have been developed [23] and will not be discussed here.

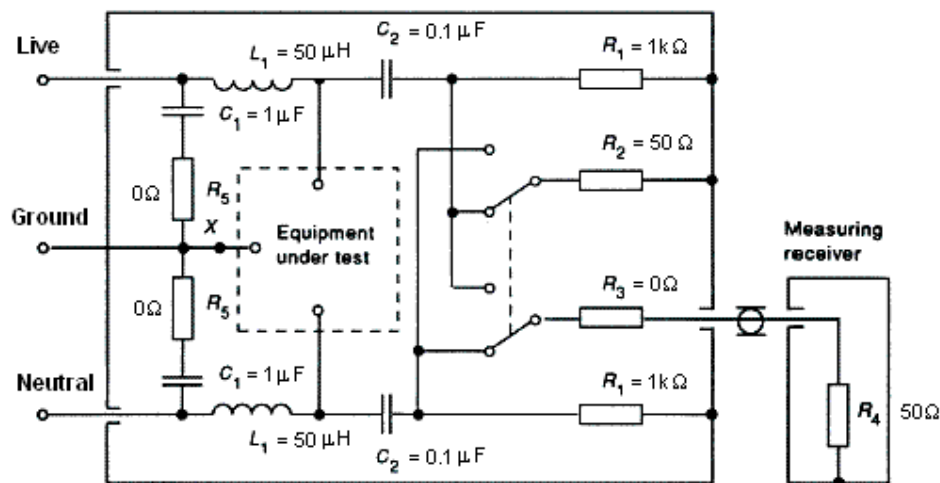


Figure 2.1 The circuit diagram of a 50 Ω / 50 μH LISN [4]

## Chapter 2 Conducted Emissions and EMI Filters in Switch Mode Power Supplies

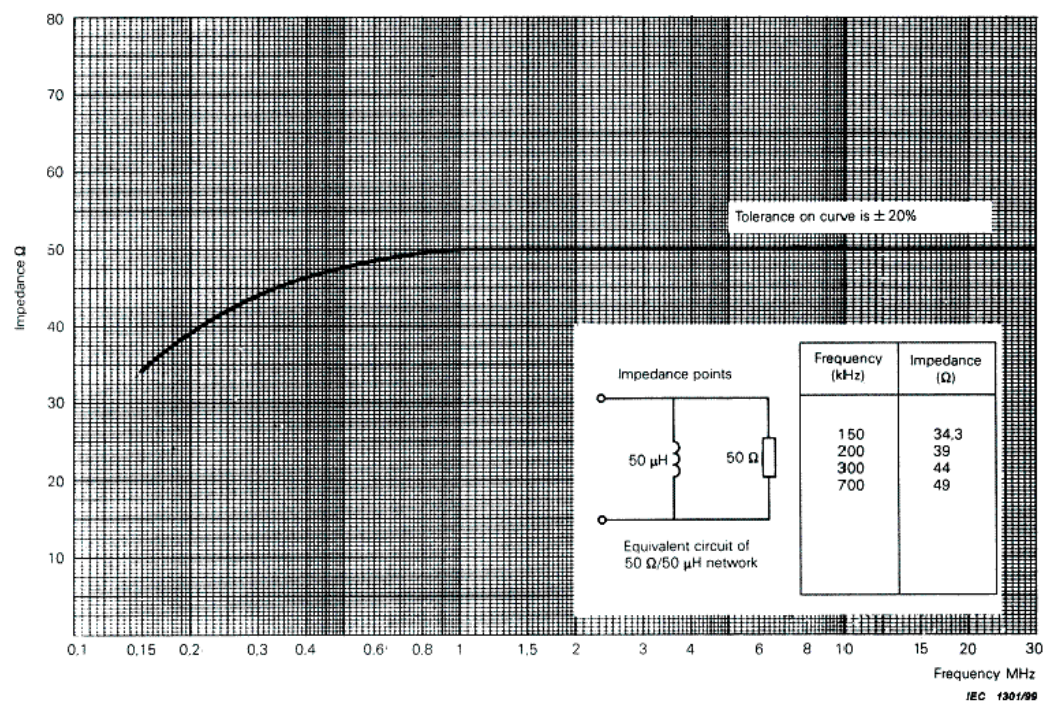


Figure 2.2 Impedance-frequency characteristic of the 50 $\Omega$ /50 $\mu$ H LISN [4]

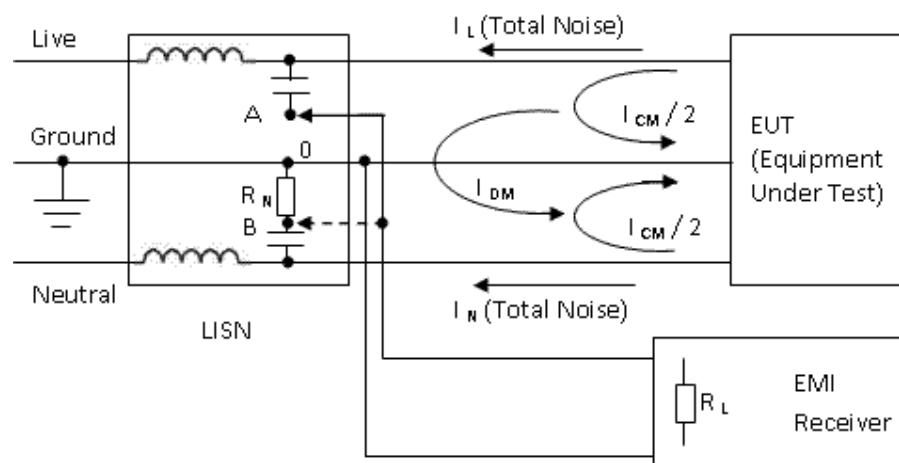


Figure 2.3 CM and DM noise currents in conducted emissions measurement setup

### **2.1.3    Conducted Emissions from Switched Mode Power Supplies**

The efficiency of switched mode power supply (SMPS) is between 60% and 90%, which is significantly higher than that of linear power supply. Typically, the efficiency of linear power supplies is of the order of 20% - 40%. SMPS is also much lighter in weight than the linear power supply. However, the high frequency switching in SMPS results in significant amount of noise spreads over a wide range of frequencies. International EMC standards restrict conducted emissions in the frequency range from 150 kHz to 30 MHz. To comply with these standards, an EMI filter is required to reduce the levels of conducted emissions produced by the SMPS below the limits. If the EMI issue is properly tackled, the merits of SMPS far out-weight the EMI problem [30].

When a SMPS is in operation, the switching elements switch on and off continuously, and repetitive voltage and current pulses are generated. Typically, the switching frequencies are from 20 kHz to several hundreds of kHz. All these voltage and current pulses generated in the power conversion switching process contribute to conducted emissions emitted by the SMPS.

The mechanism of DM and CM conducted emissions in SMPS is well reported in [2] [3] and will not be discussed here.

## **Chapter 2    *Conducted Emissions and EMI Filters in Switch Mode Power Supplies***

---

### **2.2    Power Line EMI Filters**

The advent and widespread use of SMPS has increased the concerns for controlling conducted emissions on the ac power line. The major component used in the control of conducted emission is the power line filter. Communication filters such as Bessel, Chebyshev and Butterworth, etc, are very well developed and documented. Unlike communication filters, power line filters are terminated with varying source and load impedances. In addition, the power handling requirements place constraints on the values of some filter components. For instance, a one-stage Butterworth filter with a cut-off frequency 10 kHz calls for a capacitance of 0.25  $\mu\text{F}$  and 1.13mH. Such an inductance can be easily designed for a low current rating but it may be impractical for a filter in a high-power SMPS. Hence, the EMI filter in SMPS cannot be based on the conventional communication filter design methods.

A power line EMI filter in an SMPS is a basically a low pass filter. Its objective is to reduce or eliminate high frequency (150 kHz – 30 MHz) conducted emissions generated by the SMPS without affecting the voltage and current of ac power supply frequency (50 or 60 Hz).

The difference between predicted levels of conducted EMI and the target EMI limit leads to the minimum attenuation performance required of the EMI filter. Although there are known accurate prediction methods for determining the DM noise components produced by a SMPS circuit, the CM noise components can only be

## Chapter 2 Conducted Emissions and EMI Filters in Switch Mode Power Supplies

---

estimated with approximation. Therefore, the EMI filter's DM and CM attenuations required are best determined with actual measurement results.

To determine the filter attenuation, the EMI filter's input and output terminated impedances must be known from the noise suppression point of view. The terminals connected to the noise source (SMPS or EUT) are referred to as input of the filter, and the ones connected to the ac power mains to be protected from conducted EMI constitute the filter output.

Consider the example of supplying a signal to a load as shown in Figure 2.4. The filter is inserted between the source and the load in order to prevent certain frequency components of the source from reaching the load, as shown in the Figure 2.5. Let  $P_1$  be the power received by the load when connected directly to source without the filter, and  $P_2$  be the power received by the load when the filter is inserted between the source and the load, while the input power is held constant. The load voltage without the filter inserted is denoted by  $V_1$  and the load voltage with the filter inserted is denoted as  $V_2$ . The insertion loss in dB (  $IL_{dB}$  ) of the EMI filter expressed in terms of power is defined as [59]:

$$IL_{dB} = 10 \log \left( \frac{P_1}{P_2} \right) \quad (2-1)$$

The insertion loss can also be expressed in terms of voltage as follows:

$$IL_{dB} = 20 \log \left( \frac{|V_1|}{|V_2|} \right) \quad (2-2)$$

## Chapter 2 Conducted Emissions and EMI Filters in Switch Mode Power Supplies

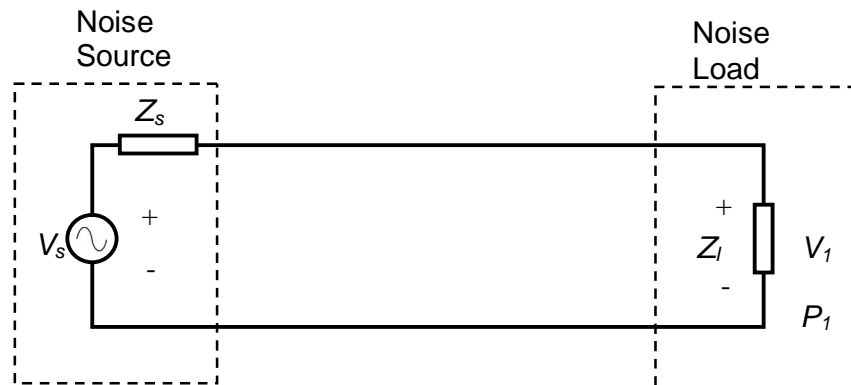


Figure 2.4 load voltage without the filter - definition of the insertion loss of a filter

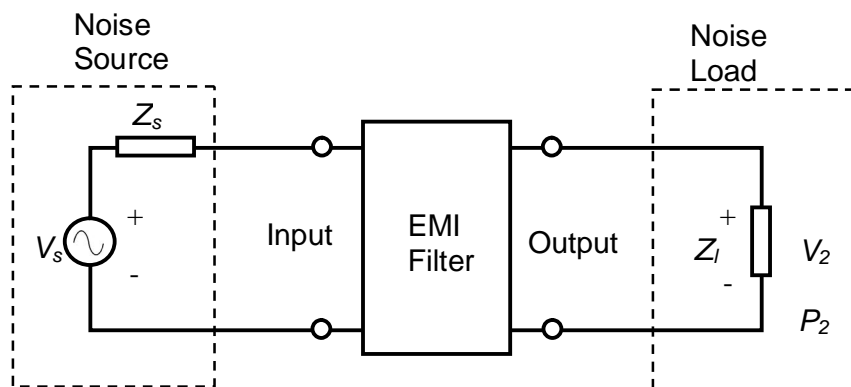


Figure 2.5 load voltage with the filter - definition of the insertion loss of a filter



## ***Chapter 2 Conducted Emissions and EMI Filters in Switch Mode Power Supplies***

---

The insertion loss of a particular filter depends on the source impedance, load impedance and the filter circuit, and therefore it cannot be stated independently of the termination impedances. Most filter manufacturers provide frequency response plots of the insertion loss of a particular filter. Usually, they assume that  $Z_s = Z_l = 50 \Omega$ . Hence, the specification of insertion loss based on  $50 \Omega$  source and load impedances may deviate from the actual applications, where the source and load impedances are not  $50 \Omega$ . For the case of SMPS in the conducted emission test setup, the terminating impedance seen by the SMPS corresponds to the  $50 \Omega$  impedance of the LISN between live and earth, as well as between neutral and earth. However, the source impedance  $Z_s$  is not  $50 \Omega$ . Hence, using the manufacturer's insertion loss data to assess the performance of the EMI filter in a SMPS may not give the correct filter insertion loss.

For cost reasons, most of the SMPS use on-board EMI filter. To achieve the expected insertion loss, the knowledge of the noise source impedance of the SMPS is very important in the design of the on-board EMI filter.

The EMI filter design methods for SMPS can be found in many publications. Almost all the design methods developed depend on the knowledge of EMI source and load impedances. In the conducted EMI measurement setup defined in standards, the load impedance of conducted EMI is that of the LISN (Line Impedance Stabilization Network), which has a well-defined and known impedance. Therefore, if the equivalent circuit model of the noise source impedance can be obtained with reasonable accuracy, the most effective filter configuration and suitable component values for the power line EMI filter of a SMPS can be designed in a systematic manner without guessing.

## ***Chapter 2 Conducted Emissions and EMI Filters in Switch Mode Power Supplies***

---

The role of EMI filter in the circuit is to minimize the conducted noise transfer over the frequency range of interest (0.15 kHz - 30 MHz), which is much higher than the operational frequency on the ac power in the circuit. This noise transfer minimization can be realized with a filter that is highly mismatched with both the source and load impedances in the frequency range of interest. Hence, to design an EMI filter with the least number of components, the need to know the noise source impedance is obvious.

A major challenge in designing cost effective power line EMI filter is to provide highest possible insertion loss in the frequency range of 0.15 MHz to 30 MHz and still capable of handling high power rating at low-frequency (50Hz/60Hz). The decision in favor of a particular filter circuit is also influenced by the input and output impedances and the limitations on the serial and parallel filter elements.

Normally, a first order filter, a filter with only one filter element, is able to meet the EMI suppression requirements when the source and load impedance are of similar impedance magnitude. A second order filter, a filter with two elements, is most useful when the source and load impedances are very dissimilar, the situation often arises in which the parallel combination of the source and load impedances is too low to be “shorted out” with a capacitor or the sum is too high for the inductor to represent a relative “open circuit”. Table 1 shows all possible combinations of source impedance  $Z_s$  and load impedance  $Z_l$ , and the most appropriate choice of filter topology. The first order and second order filters are widely used in the SMPS for conducted EMI suppression.

## Chapter 2 Conducted Emissions and EMI Filters in Switch Mode Power Supplies

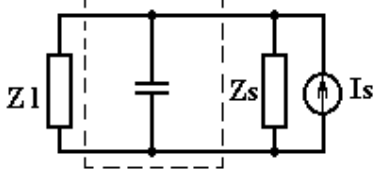
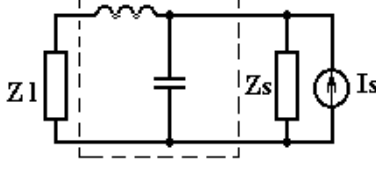
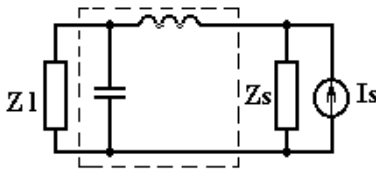
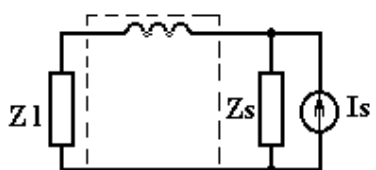
	High $Z_l$	Low $Z_l$
High $Z_s$		
Low $Z_s$		

Table 1 The first and second order filter selection matrix [2]

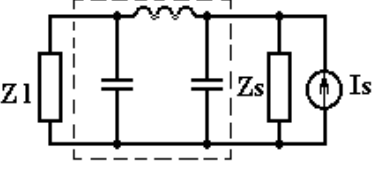
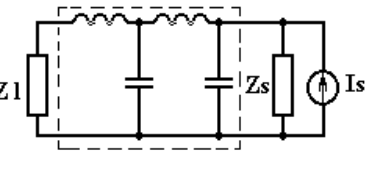
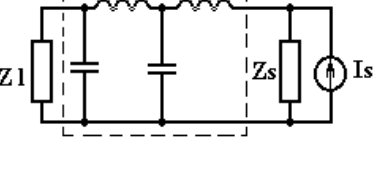
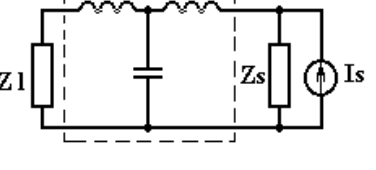
	High $Z_l$	Low $Z_l$
High $Z_s$		
Low $Z_s$		

Table 2 The higher order filter selection matrix [2]

## **Chapter 2    *Conducted Emissions and EMI Filters in Switch Mode Power Supplies***

---

In cases where the faster roll-off is required to keep the corner frequency high and, consequently, keep the components smaller than that is possible with a first or second order filter, a third or fourth order filter may be used. The most appropriate third and fourth order filter topologies versus source and load impedances are shown in Table 2. In general, the fourth and higher order filter configurations are seldom used in EMI filter design as the fast rate roll-off is not an important factor in this application. The most commonly used configurations in EMI filter design are the first, second and third order filter configurations.

### **2.3    EMI Filter Design**

Basically, EMI filter is a low pass filter, which only blocks the high frequency contents. Around the operational frequency (ac mains frequency, i.e. 50Hz or 60Hz), the EMI filter should provide negligible loss. Between the operational and the lower limit of the frequency range to be filtered (150 kHz in most cases), it must not develop resonances. Above the lower limit of the frequency range, it must provide enough insertion loss to high frequency noise.

As the conduction current paths for DM and CM currents are different, the DM and CM filters have to be designed separately. The two filters will be merged subsequently when implemented on the PCB. In EMI power line filter design, the first step is usually to design the CM filter section. Past experience shows that when CM conducted emissions are successfully suppressed below the required EMI limit; the

## **Chapter 2 Conducted Emissions and EMI Filters in Switch Mode Power Supplies**

---

DM conducted emissions are also being reduced significantly. This is due to the unintentional DM inductance offered by the leakage inductance of the CM choke and the DM shunt capacitance offered by the CM shunt capacitors. Hence, the DM filter design is always based on the DM conducted emission results after the CM filter being built in the circuit, to prevent over-designed.

### **2.3.1 CM EMI Filter Design**

As a guide, the CM filter will be designed with the following four steps:

Step 1: Determination of filter topology.

The optimal filter topology is a function of both source and load impedances. Normally, the CM filter is presented with high source impedance (capacitive in nature with small capacitance) and relatively low load impedance (about  $25\ \Omega$  due to the LISN). From the circuit diagram of LISN shown in Figure 2.1, the CM impedance of LISN seen from the EUT (Equipment Under Test) is approximately  $25\ \Omega$ , which is the result of parallel combination of  $R_2$  ( $50\ \Omega$ , the terminating resistance) and  $R_4$  ( $50\ \Omega$ , the input impedance of EMI measuring receiver). As previously discussed, the best topology that will achieve the optimum mismatch is the L-C filter with capacitor on the source side (SMPS) and the inductor facing the load side (LISN). Higher levels of

## Chapter 2 Conducted Emissions and EMI Filters in Switch Mode Power Supplies

attenuation and faster roll-off are achievable with more L-C stages. In CM filter design, multistage configuration is usually not required because the CM choke impedance can be rather high. Only in extreme cases of high source capacitance (low source impedance), it is beneficial to use a T topology, or third order filter. Hence, in most situations, a second order L-C filter is usually adequate. The CM equivalent circuit of a SMPS and the termination impedance, without any filter components, is given in Figure 2.6. The CM equivalent circuit with a second order L-C CM filter added is shown in Figure 2.7.

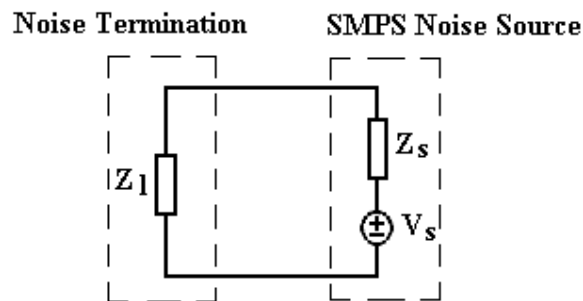


Figure 2.6 CM equivalent circuit without any filter components

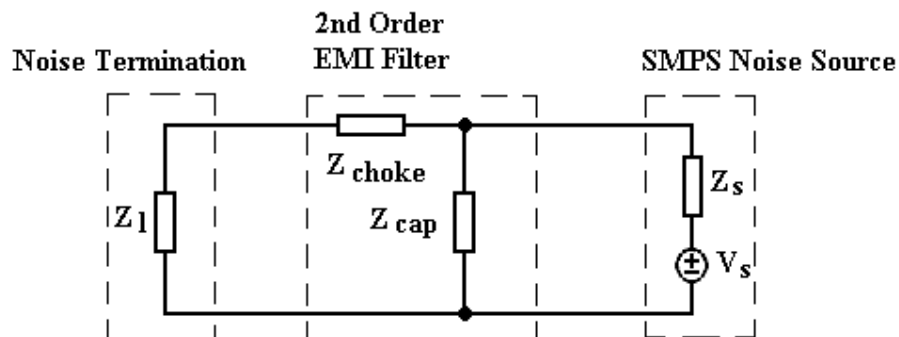


Figure 2.7 CM equivalent circuit with 2<sup>nd</sup> order CM filter

## Chapter 2 Conducted Emissions and EMI Filters in Switch Mode Power Supplies

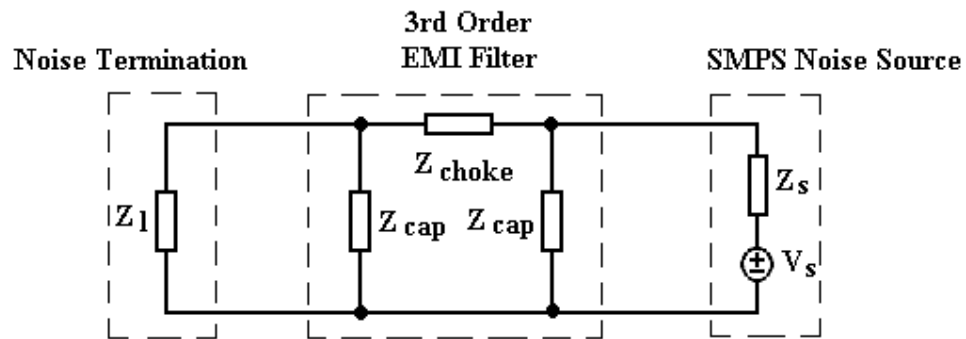


Figure 2.8 CM equivalent circuit with 3<sup>rd</sup> order CM filter

With the measurement setup defined in the EMC standards, the LISN presents the load to the EMI filter. The CM impedance of LISN is around  $25\ \Omega$  ( $50\ \Omega$  live-to-earth in parallel with  $50\ \Omega$  neutral-to-earth), which is considered as relatively low as compared to the source impedance.

The CM conducted emissions measured with LISN are the voltages across  $Z_l$  due to the noise from the SMPS.  $Z_s$  is the CM noise source impedance of the SMPS. Under the condition where no filter component is added, as shown in Figure 2.6, the CM conducted emissions are given by

$$V_{l1} = \frac{Z_l}{Z_s + Z_l} V_s \quad (2-3)$$

In the case of Figure 2.7 where the second order filter is inserted, the CM conducted emissions are given by

## Chapter 2 Conducted Emissions and EMI Filters in Switch Mode Power Supplies

---

$$V_{l2} = \frac{Z_{cap} Z_l}{(Z_l + Z_{choke})(Z_{cap} + Z_s) + Z_{cap} Z_s} V_s \quad (2-4)$$

In the case of Figure 2.8 where the third order filter is inserted, the CM conducted emissions are given by

$$V_{l3} = \frac{Z_{cap}^2 Z_l}{(Z_l Z_{cap} + Z_l Z_{choke} + Z_{cap} Z_{choke})(Z_{cap} + Z_s) + Z_{cap} Z_s (Z_l + Z_{cap})} V_s \quad (2-5)$$

The filter attenuation due to the second order filter can be calculated by

$$Att_2 = \frac{Z_{cap} (Z_s + Z_l)}{(Z_l + Z_{choke})(Z_{cap} + Z_s) + Z_{cap} Z_s} \quad (2-6)$$

Similarly, the filter attenuation due to the third order filter is given by

$$Att_3 = \frac{Z_{cap}^2 (Z_s + Z_l)}{(Z_l Z_{cap} + Z_l Z_{choke} + Z_{cap} Z_{choke})(Z_{cap} + Z_s) + Z_{cap} Z_s (Z_l + Z_{cap})} \quad (2-7)$$

With the knowledge of noise source impedance  $Z_s$ , noise load impedance  $Z_l$ , suitable values of the CM choke and shunt capacitor can be chosen to meet the attenuation requirement of the filter. The second order and the third order attenuation can be computed over the frequency range of interest with equations (2-6) and (2-7).

Step 2: Determination of targeted attenuation of the EMI filter.

Before determining the targeted attenuation of the EMI filter, designer has to alleviate the attenuation requirements by source suppression. This can be done by



## ***Chapter 2 Conducted Emissions and EMI Filters in Switch Mode Power Supplies***

---

reducing the signal amplitude and frequency, increasing the rise time and fall time of the pulse, using special EMI suppression techniques [32], etc. After the source has been reduced to as low a level as possible, the CM conducted emissions of the SMPS should be measured with no filter in place to determine the CM attenuation requirements. The difference between the conducted EMI measured and the limits specified in the standards provides the minimum attenuation requirement of the EMI filter. To establish the final requirement for EMI filter, usually a safety margin of approximately 6 to 10 dB should be added to estimated attenuation to cater for filter component tolerance.

Step 3: Determination of the capacitance of the Y capacitors.

One of the constraints on the CM filter is the limitation of the line-to-earth capacitor, commonly referred to as Y capacitor. In Figures 2.7 and 2.8, each  $Z_{cap}$  represents the resultant impedance of two parallel connected Y capacitors (one from live-to-ground and another from neutral-to-ground) for single phase ac input. A large Y capacitor would be especially effective because of the large CM noise source impedance. The upper bound on Y capacitor is imposed because of safety issues. Large Y capacitors constitute a shock hazard by creating leakage current to earth. The acceptable leakage current limits for various grounded devices are recommended by international electrical safety standards. These standards impose requirements on the maximum allowable leakage currents for a specific product, thus indirectly setting an upper limit of the Y capacitor value in the power line EMI filter.

## Chapter 2 Conducted Emissions and EMI Filters in Switch Mode Power Supplies

---

For example, Table 3 shows the maximum leakage currents of information technology equipment (ITE) defined in the relevant safety standard [57].

Table 3 Maximum leakage current defined in IEC 60950-1: 2005

Type of equipment	Terminal A of measuring instrument connected to	Maximum leakage current r.m.s.
All equipment	Accessible parts and circuit not connected to protective earth	0.25mA
Hand-Held	Equipment main protective earthing terminal (if any)	0.75mA
Movable (other than hand-held, but including transportable equipment)		3.5mA
Stationary, Pluggable Type A		3.5mA
All other Stationary Equipment.		3.5mA

The acceptable leakage current limits for certain types of medical electrical equipment defined are even more stringent because of the critical safety requirement in hospital [58]. The above-mentioned restrictions on leakage current limit the maximum value of Y capacitor that can be used in the power line filter design. As a quick estimation, the maximum value of Y capacitor can be calculated as follows [3]:

$$C_{Y,\max} = \frac{I_g}{V_m(2\pi f_m)} \times 10^6 \text{ nF}$$

## ***Chapter 2 Conducted Emissions and EMI Filters in Switch Mode Power Supplies***

---

Where  $V_m$  is the AC mains voltage in V,  $f_m$  is the mains frequency in Hz, and  $I_g$  is the maximum acceptable leakage current in mA.

Step 4: Determination of the inductance of CM choke.

The CM choke is the backbone of the CM filter. Its principle advantage is that very large inductance can be obtained on a small magnetic structure relative to the DM choke. With the knowledge of noise source impedance  $Z_s$ , noise load impedance  $Z_l$ , the maximum allowable Y capacitor and the expected attenuation of the CM EMI filter, the RF impedance of CM choke,  $Z_{choke}$ , can be computed over the frequency range of interest with equation (2-6) for the second order filter or equation (2-7) for the third order filter. With the computed CM choke impedance, suitable CM choke inductance can be selected.

Due to its relatively low self resonant frequency, the CM choke contributes attenuation mostly at lower frequencies, while the Y capacitor contributes attenuation mostly at the higher frequencies. To ensure that the filter attenuation is not degraded at the higher frequencies (up to 30 MHz), the equivalent series inductance (ESL) of the Y capacitor is of critical importance. Besides the ESL of the Y capacitor, special care should be taken to minimize the length of the leads and PCB traces and bonding between PCB ground and the metal chassis of the product.

### 2.3.2 DM EMI Filter Design

The leakage inductance of the CM choke and capacitance of Y capacitors in CM filter also contribute towards DM attenuation, though unintentionally. The DM emissions should be measured with a designed CM filter in place. In many low power applications, the CM filter has sufficient leakage inductance and shunt capacitance to adequately filter the DM emissions. In that case, design of DM filter is unnecessary. Assuming it will not, the next step is to design a DM filter for the switched mode power supply. The DM filter is also designed with 4 steps that are very similar to those steps of the CM filter design. The first step is the selection of the most appropriate filter topology. The load impedance  $Z_l$  of the DM filter is the DM termination impedance of the LISN, which is around  $100\ \Omega$  ( $50\ \Omega$  live-to-earth in series with  $50\ \Omega$  neutral-to-earth). The DM noise source of a SMPS has both a high impedance and a low impedance component. It is suggested to have a  $\pi$  filter as shown in Figure 2.9, [34].

In SMPS, the leakage inductance of CM choke is usually used as the DM suppress inductance ( $Z_{choke}$ ) in DM filter, and the two CM shunt capacitors in series are usually used as the DM shunt capacitor in DM filter ( $Z_{cap2}$ ). Therefore, the design of the  $\pi$  filter can be simplified as design of a first order filter ( $Z_{cap1}$ , one shunt capacitor before the CM choke), with DM load impedance  $Z_l$  and DM noise source impedance  $Z_{sdm}$  which consists of leakage inductance of CM choke ( $Z_{choke}$ ), two CM shunt capacitors

## Chapter 2 Conducted Emissions and EMI Filters in Switch Mode Power Supplies

in series ( $Z_{cap2}$ ) and DM noise source impedance ( $Z_s$ ) of the SMPS as shown in Figure 2.9.

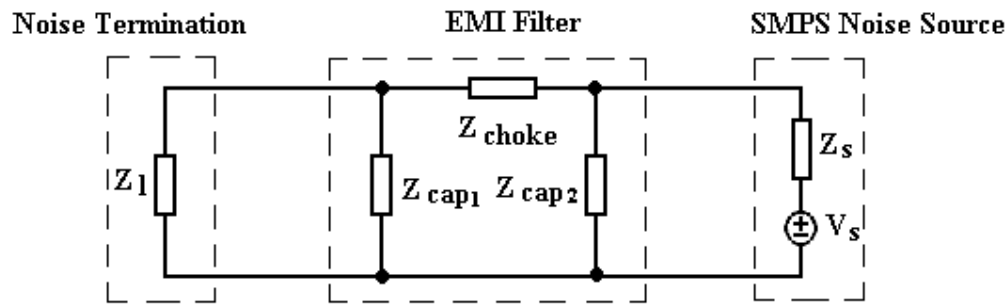


Figure 2.9  $\pi$  Filter

The second step is to determine the targeted attenuation of the DM filter. The method is the same as that for CM filter design describe above. The DM conducted emissions of the SMPS is measured with no DM filter in place (but with CM filter) to determine the DM attenuation requirements. The difference between the conducted emissions measured and the limits specified in the standards provides the DM filter attenuation required. Again, a safety margin of approximately 6 to 10 dB is added for component tolerance.

The third step is to determine the inductance of the DM inductor. In most low power applications, there is no need for the DM inductor as the leakage inductance of the CM choke gives sufficient DM inductance.

## Chapter 2 Conducted Emissions and EMI Filters in Switch Mode Power Supplies

The last step is to determine the capacitance of the X capacitors. The line-to-line capacitors in the DM filter are commonly called X capacitors. For a first order filter, the impedance of X capacitor can be computed easily.

### 2.3.3 Filter Integration

Finally, the CM and DM filters are integrated as one EMI filter in the circuit. Figure 2.10 shows a typical EMI filter circuit of a SMPS.  $L_{CM}$  is the inductance of the CM choke in the filter and  $L_{DM}$  is the leakage inductance of the CM choke which plays the role of DM inductance in the filter.  $C_X$  is the X capacitors of DM filter circuit.  $C_Y$  is the Y capacitor of the CM filter circuit. In theory, DM and CM filters are assumed to be independent to each other. In reality, some of the DM and CM filter components do affect the other noise conduction mode.

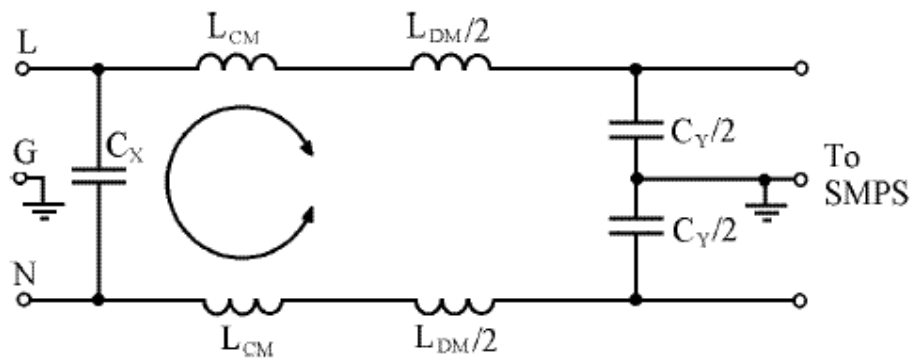


Figure 2.10 Typical EMI filter circuit of switched mode power supply

## **2.4 Insertion Loss Measurement**

Because of non-ideal behaviors of the filter elements, the actual insertion loss of the filter can differ from the calculated or expected one. The parasitic effects of the filter elements could degrade the filter performance [35]. Two filters with identical topologies and components can exhibit a significant difference in filter insertion loss due to their different layouts, undesired couplings among components and self-resonant effects of the parasitic elements. As it is impossible to predict the filter insertion with all these influences, actual measurement is still a preferred method in industry to evaluate the EMI filter performance.

### **2.4.1 No-Load 50 $\Omega$ Insertion Loss Measurement Method**

The impedances of nearly all signal generators and measuring instruments are 50  $\Omega$ . This is why most national and international standards suggest measuring the insertion loss in a 50  $\Omega$  measurement system. A test circuit to measure CM insertion loss in a 50  $\Omega$  system is shown in Figure 2.11. For this mode, the line and neutral terminals are at the same potential with respect to ground. Therefore, these two terminals are connected in parallel in the measurement setup. The insertion loss is

## Chapter 2 Conducted Emissions and EMI Filters in Switch Mode Power Supplies

measured with respect to a reference established by substituting a direct connection for the filter as shown in Figure 2.11.

For DM insertion loss, a test circuit as shown in Figure 2.12 is used. In this mode, the signals on the line and neutral terminals are the same in magnitude but opposite in phase. Therefore, the measuring circuit uses  $50\ \Omega$ ,  $180^\circ$  splitter/combiners. Again, the reference for insertion loss is determined by substituting a direct connection for the filter. The insertion loss can be worked out with equation (2-1) or (2-2) with the signal level and reference level obtained in the measurement.

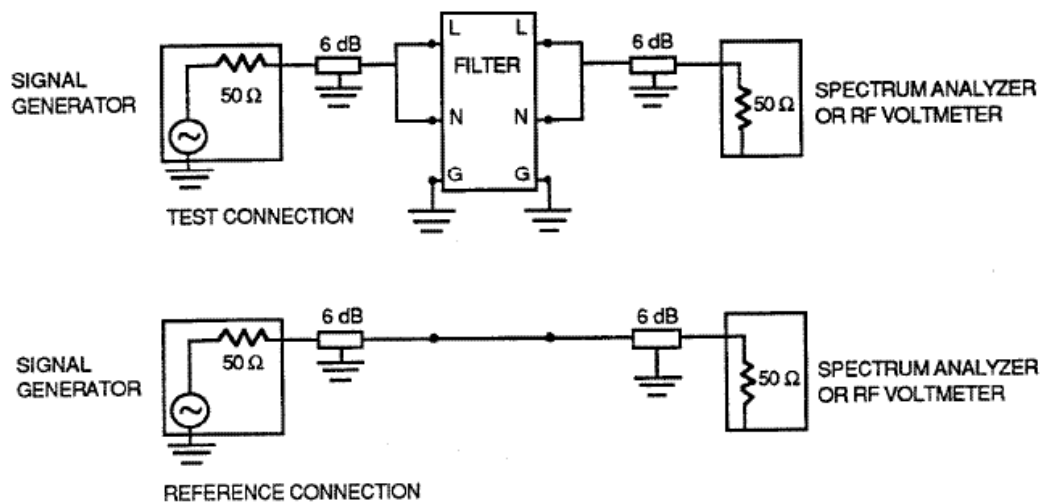


Figure 2.11 No-load  $50\ \Omega$  CM insertion loss measurement [11]



## Chapter 2 Conducted Emissions and EMI Filters in Switch Mode Power Supplies

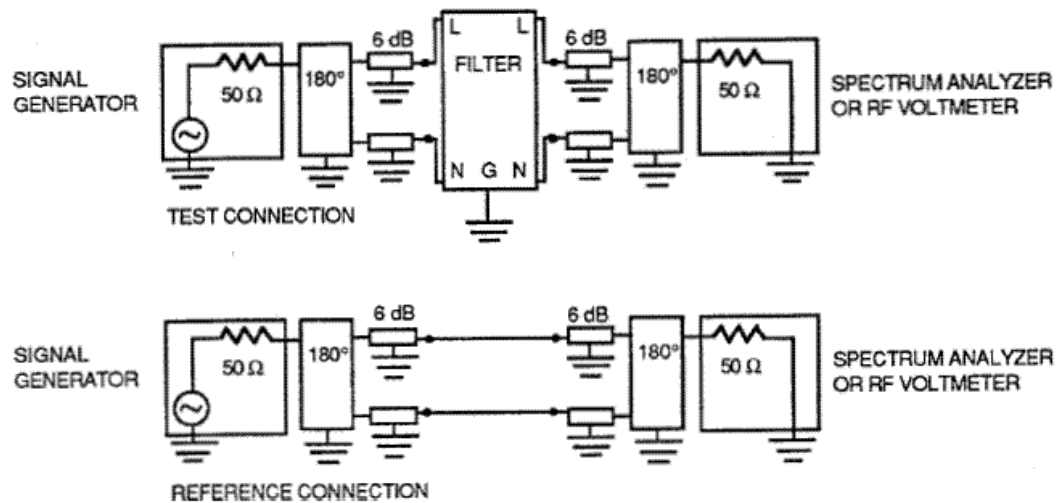


Figure 2.12 No-load 50Ω DM insertion loss measurement [11]

### 2.4.2 50Ω Insertion Loss Measurement Method With Loading

As the filter inductor could vary due to the actual load current, the previous measurement method under no load condition may over estimate the filter attenuation performance. To measure the performance of an EMI filter under loading condition, an improved test setup shown in Figure 2.13 is suggested by MIL-STD-220B. The purposes of performing insertion loss measurements under various load conditions are intended to reveal the actual choke impedance under loading condition so that the problem of incorrectly chosen choke can be rectified.

## Chapter 2 Conducted Emissions and EMI Filters in Switch Mode Power Supplies

The purpose of the RF buffer networks in Figure 2.13 is to provide RF isolation between the low frequency (operational) terminals and the measurement system; i.e. to present high impedance paths from the measurement system (signal generator, isolation attenuators, filter under test and receiver) to the DC source, and low impedance paths from signal generator to the filter under test and from the filter under test to receiver. The impedance of the isolation choke coil in the RF buffer network must be much higher in the measurement range so as not to influence the measurement accuracy. The measurement procedures of this method are similar to that of no-load  $50\ \Omega$  insertion loss measurement method mentioned earlier. The EMI filter's insertion loss can be obtained under different dc load current with an adjustable dc power source. The dc source may be replaced by a 50 Hz or 60 Hz ac power source to evaluate the filter performance under ac power condition with varying ac load currents.

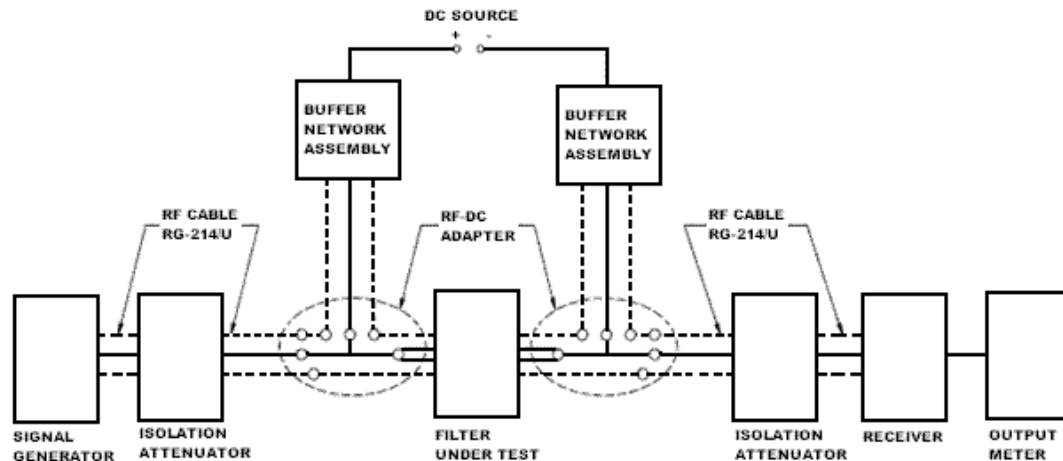


Figure 2.13 Basic test circuit for insertion loss measurement with full load [13]

## **Chapter 2    *Conducted Emissions and EMI Filters in Switch Mode Power Supplies***

---

Another international standard, CISPR 17, also suggests a similar setup of insertion loss measurement as MIL-STD-220B for evaluation of EMI filter under loading conditions, but with more source and load impedance combinations such as  $50\Omega/50\Omega$ ,  $75\Omega/75\Omega$ ,  $0.1\Omega/100\Omega$ , etc.

As discussed above, insertion loss is usually measured under clearly defined impedance conditions. However, it is well known that insertion loss is highly dependent on the load and source impedances seen by the filter. As the SMPS's noise source impedance varies in a wide range, the insertion loss obtained with above methods does not reflect the EMI filter's actual performance in SMPS.

In determining EMI filter insertion loss characteristics, it is of primary important to utilize laboratory measurement techniques whose results are indicative of actual real-world performance. To get realistic data regarding EMI filter performance under operational conditions, and to avoid over-specification of the insertion loss as a safeguard, new laboratory measurement techniques have to be developed and suggested for general use.

### **2.4.3 Worst Case Insertion Loss Measurement Method**

To study the effect of impedance mismatch conditions on the filter insertion loss, a worst case test method has been developed.

It can be shown that an insertion loss of a filter reaches a minimum for a given frequency when its input and output are matched with the complex conjugate of their

## ***Chapter 2 Conducted Emissions and EMI Filters in Switch Mode Power Supplies***

---

respective impedances [3]. In order to match such a filter configuration with the complex conjugate impedance, a choke coil of appropriate value must be inserted in series of input port and output port. The worst case insertion loss of LC configuration can be measured by placing adjustable matching capacitors on the input and an adjustable matching inductor on the output. Due to the capacitances possessed by most power line filters, it is impractical to obtain choke coils of the required value above a few MHz. But given the usual power mains impedance, laboratory measurements with a  $50\ \Omega$  system provide quick test data to approximate the worst case insertion loss values.

For determining the worst case insertion loss as a function of frequency, the minimum insertion loss must be measured at many frequencies with properly adjusted matching source impedance and load impedance. For better characterizing the EMI filters, worst case insertion loss measurement are usually made under power bias. Two test methods are employed, the serial and the parallel injection methods.

Figure 2.14 shows the series injection worst case insertion loss measuring setup. The given measuring setup serves to determine the minimum insertion loss of  $\pi$  type filter configuration, since two matching inductors are used (filter capacitors at input and output). For series injection, an ideal voltage source would be needed. The impedance associated with any realizable voltage generator must be small in relation to the equivalent series resistance of the resonant circuit at resonance. If this condition is not met, degradation in Q-factor occurs, and the worst case insertion loss cannot be determined. Usually, a few  $\text{m}\Omega$  of equivalent series resistance is required. To obtain such a low value, a voltage injection probe must be used. The voltage injection probe must have a large turn ratio and often must be terminated by low resistance.

## ***Chapter 2 Conducted Emissions and EMI Filters in Switch Mode Power Supplies***

---

Furthermore, the inductance inserted by the voltage injection probe (as well as current detection probe) must be minute, since it limits the highest interface resonance frequency that can be attained with a given EMI filter. This condition requires very tight coupling between the two probe windings. With special wound probe, about 50 mH equivalent series inductance can be achieved.

Because of parasitic inductances, the worst case insertion loss can be measured only up to the MHz range with series injection. The upper limit of the measurement frequency range can be increased by parallel injection. The measuring setup of worst case insertion loss with parallel injection is shown in Figure 2.15. The most important benefit of the parallel injection method is that no inductive injection probe is needed, since the injection is made by a high pass network that keeps the low frequency biasing voltage off the current source and detector. This network is represented by the coupling capacitor,  $C$ , in Figure 2.15. To establish a characteristic interfacial resonance, it is essential that the current source and the detector have a large resistance compared to the resistance of the resonant circuits on the input and output at resonance. Typically, a  $50\ \Omega$  current source and detector is large enough for parallel injection worst-case insertion loss measurement. The upper measurement frequency limit will be determined by various parasitic inductances. In general, an upper limit of about 10 MHz can be expected. The lower measurement frequency limit for both serial and parallel injection will be affected by the size of the matching choke coil and the  $10\ \mu\text{F}$  capacitor needed for high frequency isolation. As an example, the lower measurement frequency limit does not exceed the 20 kHz when the measurement is made with instrument of  $R = 50\ \Omega$ , assuming an average filter capacitance of  $2\ \mu\text{F}$  and a Q-factor of 10 for the matching choke coil.

## Chapter 2 Conducted Emissions and EMI Filters in Switch Mode Power Supplies

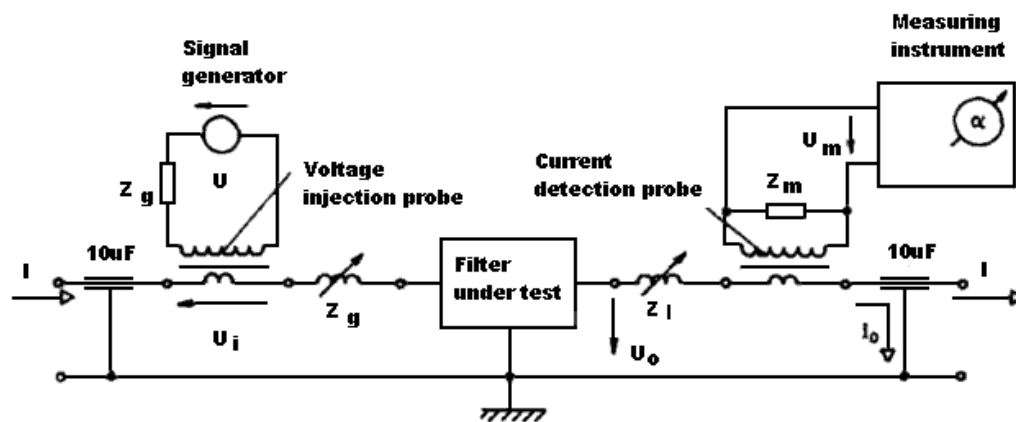


Figure 2.14 Series injection worst case insertion loss measurement system [3]

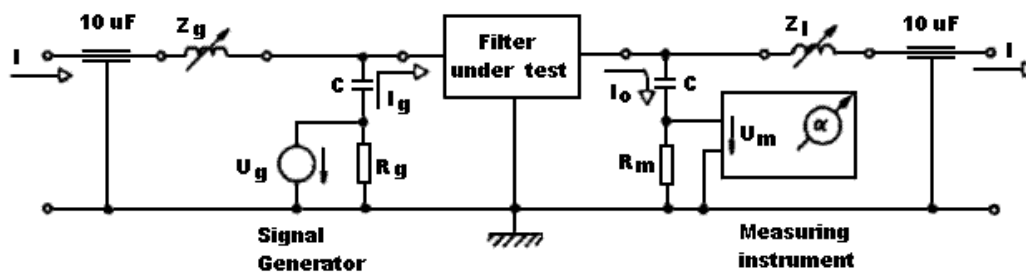


Figure 2.15 Parallel injection worst case insertion loss measurement system [3]

## **Chapter 3 Two-Current-Probe Method**

### **3.1 Introduction**

In the previous chapter, the various methods of filter insertion loss have been discussed. However, to accurately predict the filter attenuation performance, the equivalent CM and DM noise source impedances of the SMPS must be known. To determine the noise source impedance of the SMPS under the actual power-up condition, a two-current-probe measurement approach is proposed.

The concept of measuring unknown impedance using the two-current-probe method with a network analyzer was first reported for ac power mains impedance measurement. Nicholson and Malack [20] conducted the impedance measurement of ac mains outlets in the United States using the two-current-probe method in the frequency range from 20 kHz to 30 MHz. This measurement technique was also studied by Southwick and Dolle [21]. The measurement made in the United States was later compared with the similar measurement performed in Europe [36]. Schlicke [54] presented statistical data collected from many hundreds of outlets in households, factories, laboratories, aboard naval vessels, and others, in the frequency range from 1 kHz to 10 MHz. Several other authors investigated power line impedances for various purposes in different frequency range with the two-current-probe method in 1980's.

Vines et al. [37] described measurement results and an analysis of impedance of residential power-distribution circuit at frequencies from 5kHz to 20 kHz in 1985. These frequencies were used by systems such as distribution-line carriers that employed the power distribution circuit as a communication medium. With the aim of investigating surge and “high frequency” propagation, Martzloff and Gauper measured the input impedance of industrial power lines over the frequency range of 100 Hz – 10 MHz [38]. Investigating the possibility of using power lines as small scale local area networks (LAN), Tanaka made measurement of power line impedances over frequency range of 20 kHz – 30MHz [39]. Forti and Millanta, surveying the origin of the low frequency oscillatory transients, measured power line impedances from DC to 20 kHz [40]. Kwasniok extended the frequency range of the two-current-probe method up to 500 MHz in his measurement of power line impedances in 1993 [22]. For many years, there has been continuing interest to use the two-current-probe method in the impedance measurement of ac power-main distribution networks and in the monitoring of the quality of the ac power-main voltage. Tanaka measured the transmission characteristic of power lines used for data communication in the frequency range up to 500MHz [41]. See, Kamarul, and So also made used of this two-current-probe method in characterizing the power line communication networks [42].

In this thesis, with a modified measurement setup, the two-current-probe method is extended to characterize the CM and DM RF noise impedances of SMPS as well as impedance of EMI suppression chokes under actual operating conditions.

In the measurement, one current probe is used as an injection probe and another current probe is used as a receiving probe, the unknown impedance is characterized



with analysis based on the injected signal level and received signal level. With a pre-measurement calibration process, all parasitic effects in the measurement setup in the given frequency range of interest can be eliminated. The measurement results collected allows EMI filter designers to obtain the CM and DM noise source impedances of any SMPS in normal operating conditions as well as to assess the EMI suppression performance of EMI suppression chokes (CM and DM chokes) under realistic loading conditions with reasonable accuracy.

### 3.2 Theoretical Background

To illustrate the concept of the two-current-probe method, Figure 3.1 shows the basic measurement setup to measure any unknown impedance  $Z_X$ . The basic instruments involved consist of an injecting current probe, a receiving current probe and a network analyzer. The two probes and the coupling capacitor form a coupling circuit to avoid direct connection to  $Z_X$ , which may be a part of a high-voltage, high-current circuit. Port 1 of the network analyzer induces a signal in the coupling loop through the injecting current probe. Port 2 of the network analyzer measures the resultant circulating current in the coupling loop with the receiving current probe.

Figure 3.2 shows the equivalent circuit of the measurement setup.  $V_1$  is the output signal source voltage at port 1 connected to the injecting probe and  $V_2$  is the resultant signal voltage measured at port 2 with the receiving probe.  $Z_{p1}$  and  $Z_{p2}$  are output and input impedances of ports 1 and 2, respectively, which are usually  $50\ \Omega$ .  $L_1$  and  $L_2$  are

the primary self-inductances of the injecting probe and receiving probe, respectively; and  $L$  is the self-inductance of the coupling loop.  $M_1$  is the mutual inductances of injecting probe and the coupling loop,  $M_2$  is the mutual inductance between the receiving probe and the coupling loop. By reflecting the primary circuits of the injecting probe and receiving probe in the coupling circuit loop, the simplified equivalent circuit of the measurement setup is illustrated in Figure 3.3.

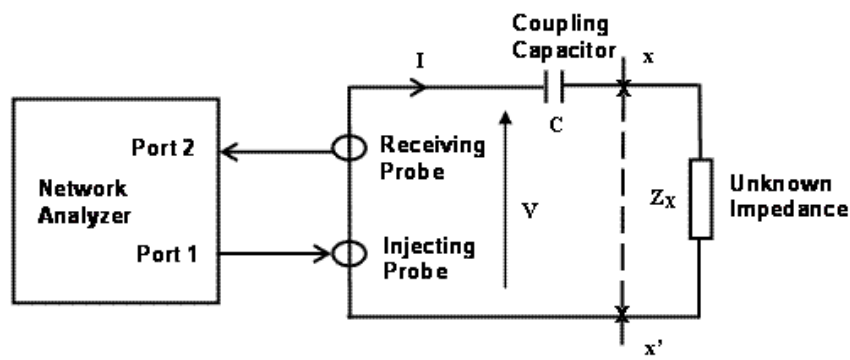


Figure 3.1 Basic setup of the two-current-probe method with network analyzer

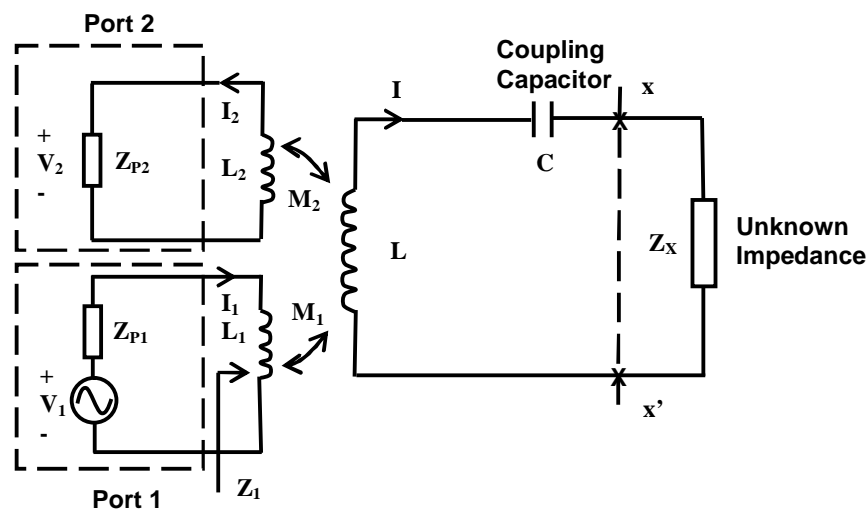


Figure 3.2 The equivalent circuit of the two-current-probe measurement setup

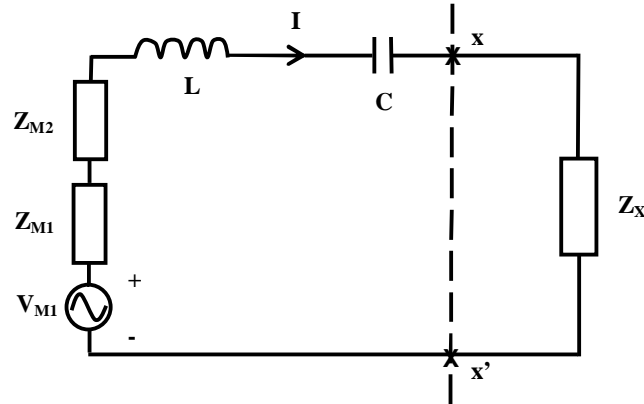


Figure 3.3 Simplified equivalent circuit of the two-current-probe measurement setup

The resultant current in the coupling loop due to the injecting signal is given by

$$I = \frac{V_{M1}}{Z_{M1} + Z_{M2} + j\omega L + \frac{1}{j\omega C} + Z_X} \quad (3-1)$$

$$\text{where } Z_{M1} = \frac{(\omega M_1)^2}{Z_{p1} + j\omega L_1}, \quad Z_{M2} = \frac{(\omega M_2)^2}{Z_{p2} + j\omega L_2} \quad \text{and} \quad V_{M1} = j\omega M_1 \left( \frac{V_1}{Z_{p1} + Z_1} \right).$$

Finally, the coupling circuit can be replaced by an equivalent voltage source  $V_{M1}$  in series with an equivalent source impedance  $Z_{setup}$ , where  $Z_{setup} = Z_{M1} + Z_{M2} + j\omega L + 1/j\omega C$ . So equation (3-1) can be rewritten as

$$I = \frac{V_{M1}}{Z_{setup} + Z_X} \quad (3-2)$$

From equation (3-2), the unknown impedance  $Z_X$  can be obtained by

$$Z_X = \frac{V_{M1}}{I} - Z_{setup} \quad (3-3)$$

The current  $I$  measured by the receiving probe can be determined by:

$$I = \frac{V_2}{Z_{T2}} \quad (3-4)$$

where  $Z_{T2}$  is the calibrated transfer impedance of the receiving probe.

Substituting  $V_{M1} = j\omega M_1 \left( \frac{V_1}{Z_{p1} + Z_1} \right)$  and equation (3-4) into equation (3-3) leading to

$$Z_X = \left( \frac{j\omega M_1 V_1}{Z_{p1} + Z_1} \right) \frac{Z_{T2}}{V_2} - Z_{setup} \quad (3-5)$$

Let  $k = \frac{j\omega M_1 Z_{T2}}{Z_{p1} + Z_1}$ , then equation (3-5) can be expressed as

$$Z_X = \frac{kV_1}{V_2} - Z_{setup} \quad (3-6)$$

By maintaining  $V_I$  at a fixed magnitude,  $kV_I$  is a frequency-dependent constant. If  $Z_X$  is replaced with a known precision standard resistor  $R_{std}$ , the constant coefficient  $kV_I$  can be determined by

$$kV_I = (R_{std} + Z_{setup}) V_2 \big|_{Z_X = R_{std}} \quad (3-7)$$

If  $Z_X$  is replaced with a short circuit, one gets

$$kV_I = Z_{setup} V_2 \big|_{Z_x=0} \quad (3-8)$$

From equations (3-7) and (3-8), the impedance due to the coupling circuit  $Z_{setup}$  can be obtained through:

$$Z_{setup} = \frac{V_2 \big|_{Z_x=R_{std}}}{V_2 \big|_{Z_x=0} - V_2 \big|_{Z_x=R_{std}}} R_{std} \quad (3-9)$$

Once  $Z_{setup}$  is found, the coupling circuit is ready to measure any unknown impedance  $Z_X$  as follows

$$Z_X = \frac{kV_I}{V_2 \big|_{Z_x=unknown}} - Z_{setup}$$

$$Z_X = \frac{(R_{std} + Z_{setup}) V_2 \big|_{Z_x=R_{std}}}{V_2 \big|_{Z_x=unknown}} - Z_{setup} \quad (3-10)$$

In most practical situations,  $Z_{setup}$  is small and can be neglected. Then, equation (3-10) can be simplified to

$$Z_X = \frac{R_{std} V_2 \big|_{Z_x=R_{std}}}{V_2 \big|_{Z_x=unknown}} \quad (3-11)$$

However, if the unknown impedance  $Z_X$  to be measured is small and comparable to  $Z_{setup}$ , then  $Z_X$  must be evaluated according to equation (3-10) to ensure good measurement accuracy.

In the measurement,  $V_1$  and  $V_2$  are the voltages at the terminals of the injecting probe and receiving probe, respectively. These voltages are related to the S parameters measured with the network analyzer since  $V_1 = V_{1 \text{ forward}} (1 + S_{11})$ , and  $V_2 = V_{1 \text{ forward}} S_{21}$ . Hence:

$$\frac{V_2}{V_1} = \frac{S_{21}}{1 + S_{11}} \quad (3-12)$$

Here the  $S_{11}$  is measured at the terminal of injecting probe with the receiving port (Port 2 of the network analyzer) connected to the receiving probe.  $S_{11} = 0$  when the impedances at Port1 and the impedances at port 2 are matched, respectively.

In the actual measurement, the input impedances of the current probes available are  $50 \Omega$ . As the impedance is quite well matched between the probes and the network analyzer's ports, we can say that  $S_{11} \approx 0$ , hence,  $V_1 \approx V_{1 \text{ forward}}$  and  $V_2 \approx V_1 S_{21}$  all the time.

### 3.3 Measurement Setup with a Spectrum Analyzer and a Signal Generator

Most researchers prefer to using the network analyzer in their measurement of ac mains RF impedance with the two-current-probe method, as the measured results provide the both magnitude and phase of the RF impedance under measurement. This is usually not an issue when the RF background noise level is relative low. However, to measure the true RF impedance while the SMPS is powered up for the purpose of

the filter design, the built-in power line filter of the SMPS is not present. Hence, conducted emissions in the frequency range of 150 kHz to 30 MHz, can be very high and network analyzer may not be able to track the injected signal properly. When the measurement with the two-current-probe method is employed on a SMPS in its actual operating conditions, the useful induced signal from the injecting probe may be masked by the RF back ground noise mentioned. The network analyzer, which is based on tracking the useful injected signal, may not be able to identify and track the correct signal, and hence, meaningful measurement in certain frequency ranges due to these background RF noise may be impossible. The alternative approach of the two-current-probe method for the measurement of RF impedance under noisy background noise is to replace the network analyzer with a signal generator and a spectrum analyzer in the measurement.

Figure 3.4 shows the basic setup of the two-current-probe method with a spectrum analyzer and a signal generator. The signal generator produces the RF signal to be injected into the electronic circuit under measurement with the injecting probe. By adjusting the output signal level of the signal generator to a sufficient level at the selected frequency points, the induced signal from the injecting current probe, will have a better signal to noise ratio, so that it can be easily detected by the spectrum analyzer via the receiving current probe.

The measurements are made at sufficient selected frequencies that cover the required frequency range. However, using the signal generator and spectrum analyzer measurement setup, only the magnitudes of injected signal  $V_1$  (signal generator output level) and the received signal  $V_2$  (reading of spectrum analyzer) are obtained at the selected frequency points. The magnitude of unknown impedance can be obtained with

equation (3-10) or (3-11) based on measured  $V_1$  and  $V_2$  and pre-calibration results. By observing the trend of the measured impedance's magnitude with frequency (flat, +20 dB/decade or -20 dB/decade), a reasonably accurate impedance model in terms of resistor, inductor and capacitor can be derived for the unknown impedance.

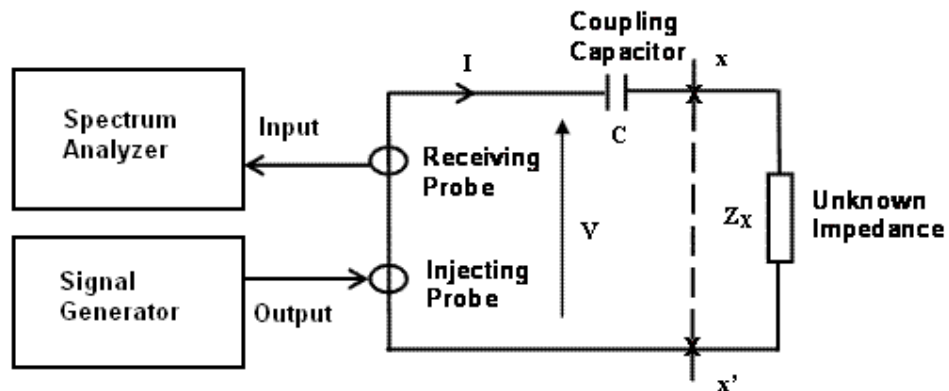


Figure 3.4 Measurement setup with a spectrum analyzer and a signal generator

The measurement process with this measurement setup may be tedious as the measurement is made point by point in the interested frequency range, especially when the measurement frequency range is wide with a few hundreds of frequency measurement points. In order to speed up the measurement process, tracking signal generator, either internal tracking signal generator module of the spectrum analyzer or external tracking generator, is recommended in this measurement. Figure 3.5 shows the



basic setup of the two-current-probe method using spectrum analyzer with an internal tracking signal generator module.

In the frequency range where the induced signal can be clearly differentiated from the background RF noise, the measurement can be performed with data acquisition software to capture the data in the frequency range via a PC connected to the spectrum analyzer. The whole measurement process takes a few seconds for the full frequency range of 150 kHz to 30 MHz. In the frequency range where the induced signal is masked by the background RF noise in the electronic circuit, one could increase the injected signal level by increasing the tracking signal generator's output level. Another effective countermeasure is to skip the measurement in some narrow frequency bands where the background RF noise is too high, and characterize the unknown impedance with data obtained just before and after the narrow frequency band.

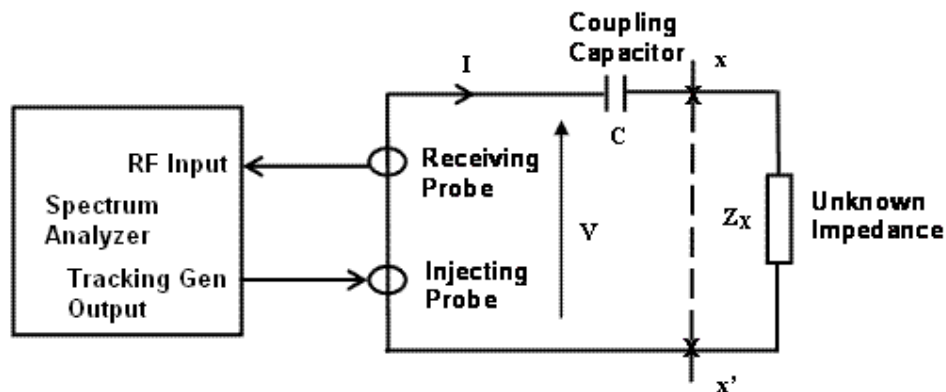


Figure 3.5 Setup using a spectrum analyzer with an tracking signal generator module

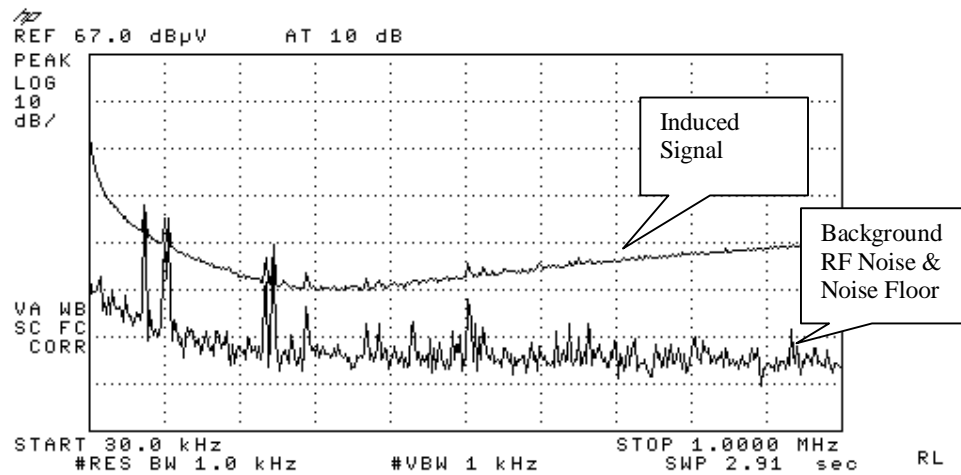


Figure 3.6 Induced signal and background RF noise

Figure 3.6 shows an induced signal and background RF noise captured with the data acquisition software during the measurement. Besides a few high magnitude narrow band RF background noises was detected, very good signal to noise ratio is maintained in the frequency range of interest. For the narrow frequency bands where high magnitude RF background noises are detected, one can just simply skip the data in these narrow frequency bands and work out the impedance values of the unknown impedance in the rest of the frequency range with equations derived above. The unknown impedance is still able to be characterized in these narrow frequency bands with the impedance values just before and after the narrow frequency band. The data captured with the data acquisition software is in “.xls” format (Microsoft Excel file), which makes data process easier and faster.

### 3.5 Validation

In order to validate the proposed measurement method, Tektronic CT-1 (5 mV/mA, bandwidth 25 kHz to 1000 MHz) and CT-2 (1 mV/mA, bandwidth 1.2 kHz to 700 MHz) current probes are chosen as the injecting probe and receiving probe, respectively. The HP 8591E spectrum analyzer with an internal tracking signal generator module is employed for the measurement. The data acquisition was performed with “HP Benchlink” software at an IBM notebook PC connected to the spectrum analyzer with GPIB cable. Two 1  $\mu$ F capacitors connected in parallel are used as the coupling capacitor. Figure 3.7 shows the measurement setup used in the validation.

To obtain the frequency-dependent coefficient  $kV_I$  for the two probes measurement setup, a precision resistor  $R_{std}$  ( $600 \Omega \pm 1\%$ ) is measured using the two probes setup. After that, without any resistor ( $Z_X = 0 \Omega$ ), the measurement is repeated. The impedance due to the coupling circuit  $Z_{setup}$  is obtained with  $V_2/Z_X=R_{std}$ ,  $V_2/Z_X=0$  and  $R_{std}$ , in accordance with equation (3-9). Once  $kV_I$  and  $Z_{setup}$  are found, the coupling circuit is now ready to measure any unknown impedance. For validation purposes, a few resistors of known values are treated as unknown resistors and measured using the proposed method. Figure 3.8 shows the measurement results with the two-current-probe method for resistors with resistance value 1 k $\Omega$ , 5 k $\Omega$  and 10 k $\Omega$ . It can be seen the measured resistance is in close agreement with the stated resistance of these resistors. For 5 k $\Omega$  and 10 k $\Omega$  resistors, the roll off above 10 MHz is expected due to

the parasitic capacitance that is inherent to resistors of large resistance. For comparison purposes, the magnitude of  $Z_{setup}$  is also plotted in Figure 3.8. Based on the trend of impedance variation with frequency, the impedance of the coupling circuit  $Z_{setup}$  is capacitive in nature at low frequency because of the coupling capacitors. However, it becomes more inductive as frequency increases, which is due to the loop inductance of the coupling circuit. The inductive reactance can be as high as  $40\ \Omega$  at 30 MHz. Hence, if the unknown impedance to be measured is low, it should be measured and determined in accordance with equation (3-10) so that  $Z_{setup}$  can be eliminated for better measurement accuracy.

For resistors with resistance  $2\ \Omega$ ,  $5\ \Omega$ ,  $10\ \Omega$  and  $25\ \Omega$ , the impedance due to the coupling circuit cannot be ignored and  $Z_{setup}$  has to be subtracted from the measurement results for better accuracy. By subtracting  $Z_{setup}$  from the measurement results, the measured resistance has agreed very well with the stated resistance of these resistors, as demonstrated in Figure 3.9. Hence, the pre-measurement characterization of the measurement setup serves as a good mean to eliminate measurement error due to the coupling circuit.

To further validate the accuracy of the two-current-probe method, the  $5\ \text{k}\Omega$  and  $5\ \Omega$  resistors are measured again using the HP 4191A impedance analyzer. The comparisons of measured results using the two-current-probe method and the HP4191A impedance analyzer for  $5\ \Omega$  and  $5\ \text{k}\Omega$  resistors are given in Figure 3.10 and Figure 3.11, respectively. As the lowest operating frequency of the HP 4191A is 1 MHz, only measured results from 1 MHz to 30 MHz are compared. The measured results using the two-current-probe method show good agreement with those obtained

from the HP 4191A. Using the results of the HP4191A as references, the maximum deviations are less than 5% and 10% for 5 k $\Omega$  and 5  $\Omega$  resistors, respectively.

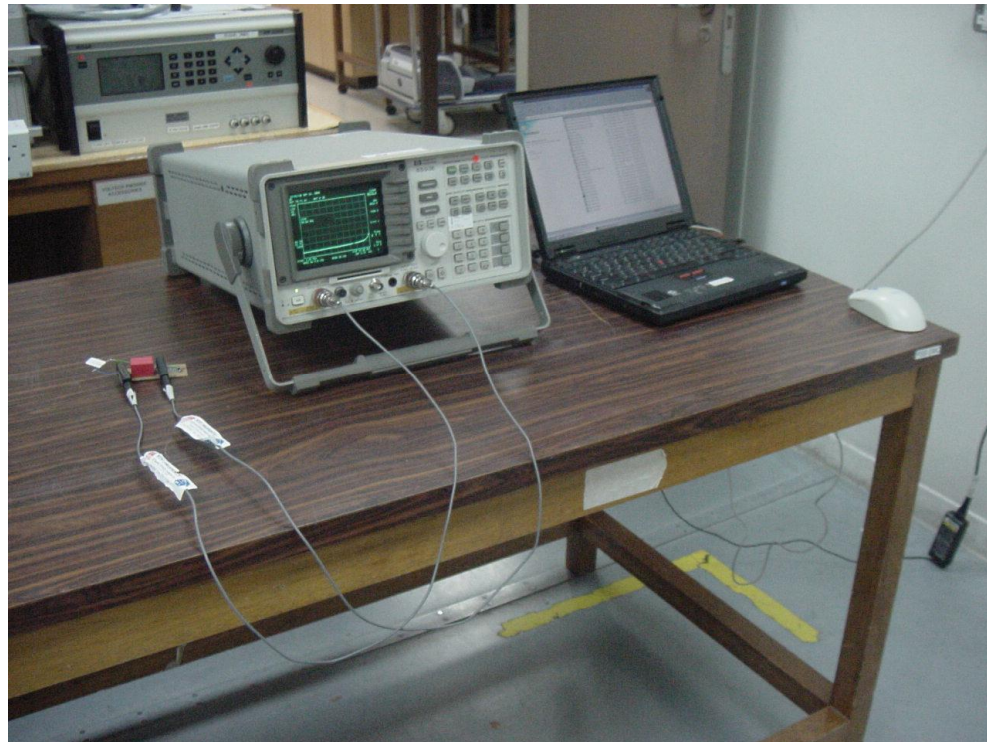


Figure 3.7 Measurement setup in validation

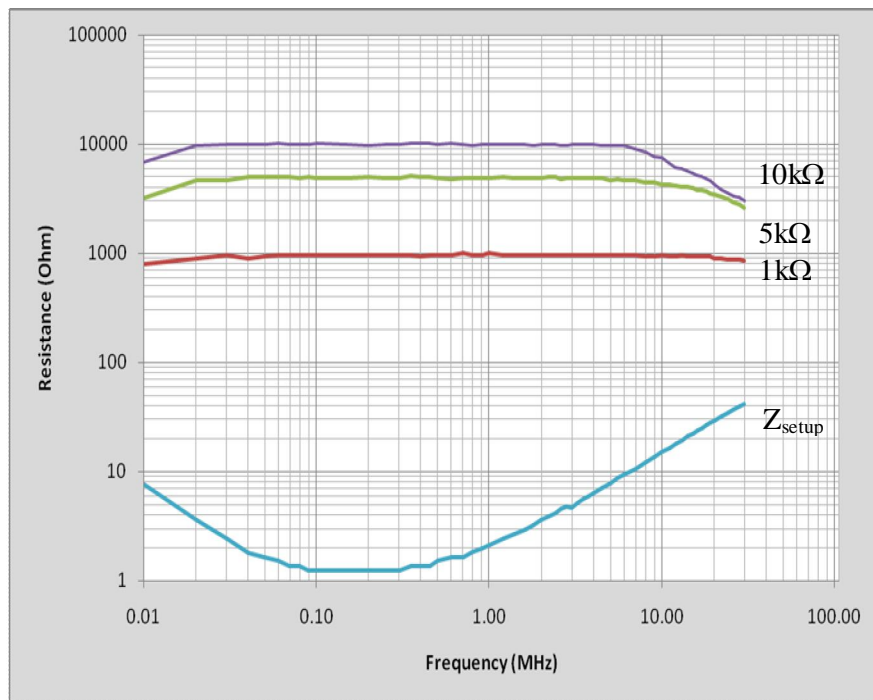


Figure 3.8 Measurement of large-resistance resistors

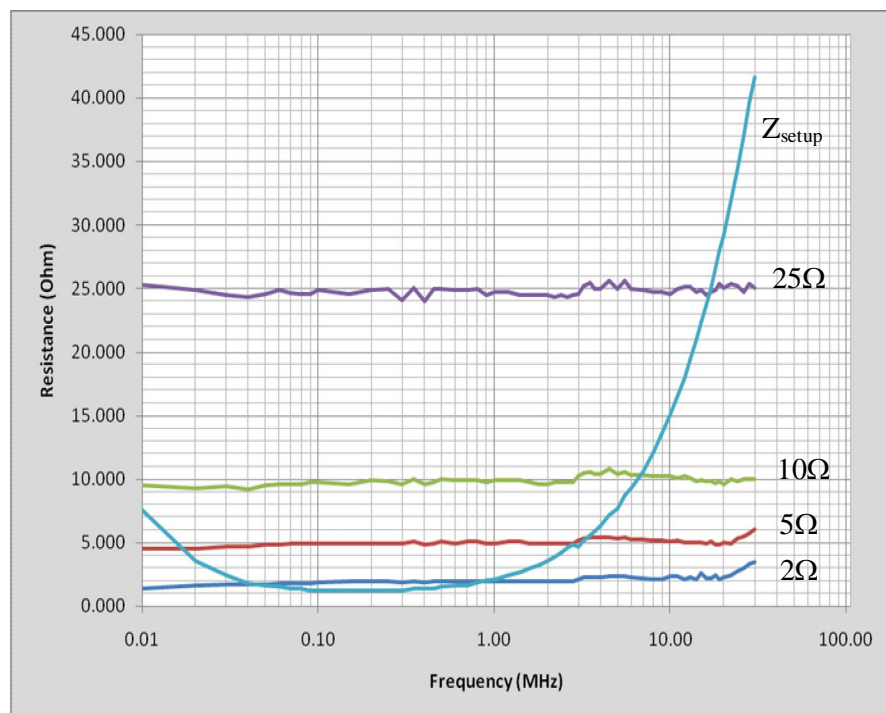


Figure 3.9 Measurement of small-resistance resistors

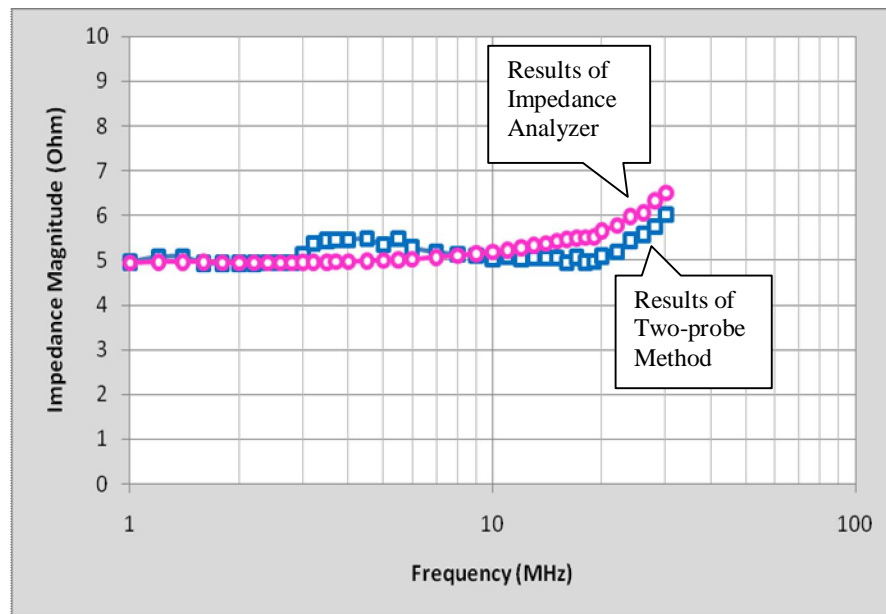


Figure 3.10 Comparison of measured results for 5  $\Omega$

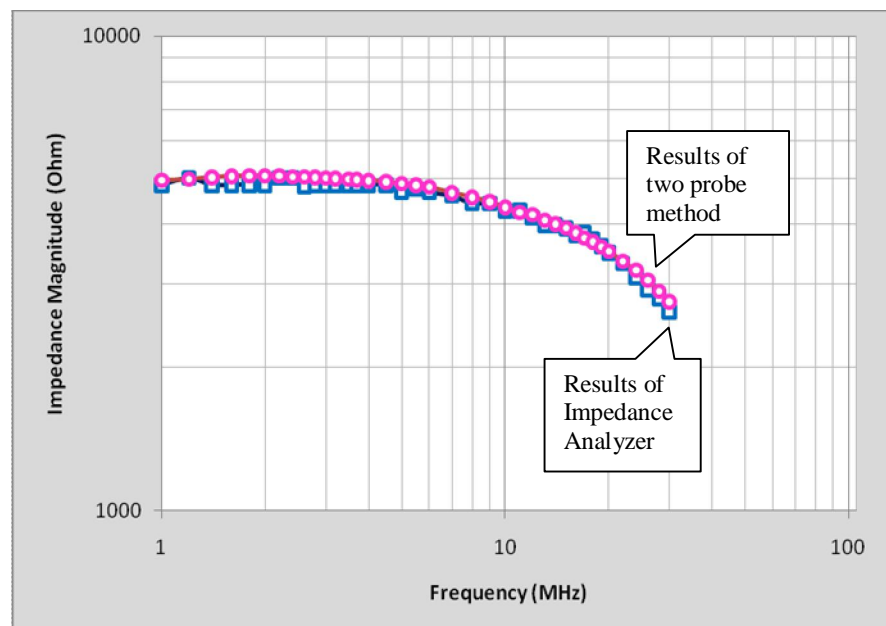


Figure 3.11 Comparison of measured results for 5 k $\Omega$

As a final check, the two-current-probe measurement using a spectrum analyzer with an internal tracking signal generator module is compared with that using a vector network analyzer. An inductor is chosen as component-under-test. By using an RF impedance analyzer HP 4396B, the equivalent circuit of the inductor is found to be a circuit consists of an inductor ( $L \approx 136.24\mu\text{H}$ ) and a resistor ( $R \approx 8.21\Omega$ ) in series, parallel with a capacitor ( $C \approx 1.71\text{pF}$ ). The first approach uses a spectrum analyzer with an internal tracking signal generator module and the second approach makes use of a Rohde & Schwarz ZVB vector network analyzer (VNA). Figure 3.12 shows the comparison of measured impedance magnitudes obtained based on the two approaches. Close agreement between the measured results from the two approaches is observed. It is also noticed the spectrum analyzer measurement approach provides much stable measured data as one could observe and increase the injecting signal level, where necessary, during the measurement so as to provide good signal to noise ratio. As the measurement using VNA is based on auto-tracking, care should be exercise to ensure that the tracking signal source from the VNA is strong enough to obtain stable reading.



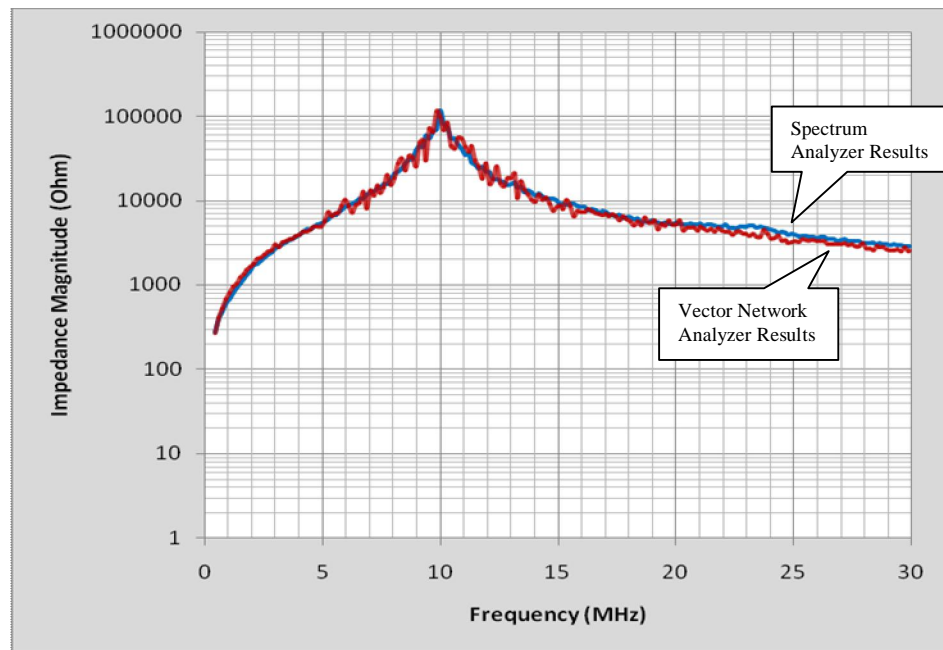


Figure 3.12 Comparison of results obtained with spectrum analyzer (blue curve) and vector network analyzer (brown curve)

## **Chapter 4      Measurement of Noise Source**

### **Impedance of SMPS**

#### **4.1    Noise Source Impedance of SMPS**

The knowledge of noise source impedance and termination impedance of a switched mode power supply (SMPS) is essential in its power line EMI filter design, especially in the selection of filter circuit topology and filter components' value. EMI filter performance depends not only on the filter itself but also the noise source impedance of the circuit and the noise load impedance at the test site. The filter design guideline is to maximize impedance mismatch so that the noise energy delivered to the load is minimized. As typical conducted emissions measurement setup requires a line impedance stabilization network (LISN), both the CM and DM termination impedances seen by the SMPS are well defined in the standards. However, the characteristics of CM and DM noise source impedances of the SMPS over the EMI regulated frequency range of 150 kHz to 30 MHz are not readily available.

Shih etc. have found that under some assumptions the attenuation of a filter has little to do with the noise source impedance [45]. Their approach simplifies the filter designing procedure but is valid only for a particular filter topology under certain

conditions. In addition, the approach cannot predict filter resonance performance. To solve the problems mentioned above, EMI noise source impedance has to be known.

Due to the conduction modes of a SMPS, it is essential to determine the noise source impedance  $Z_s$  in separate conduction modes, namely, in terms of the CM noise source impedance  $Z_{scm}$ , and the DM noise source impedance  $Z_{sdm}$ . The definition is given as follows.

CM source impedance is the impedance between the new terminal formed by shorting line and neutral together, and the terminal ground, when looking into the SMPS. See Figure 4.1. The major components of CM noise source impedance are the unintentional capacitance between the switching device and its heatsink, the parasitic capacitance between the heatsink and the grounded chassis, and the parasitic capacitances between other devices or wires, which carry pulsating voltage waveform and the grounded chassis.

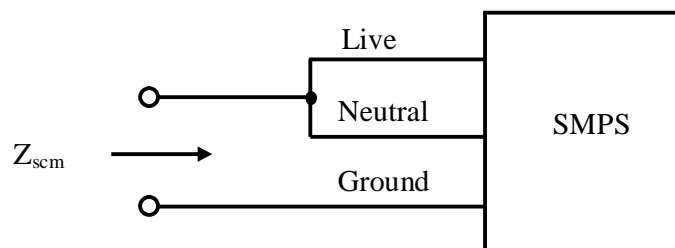


Figure 4.1 CM source impedance of SMPS

**Chapter 4****Measurement of Noise Source Impedance of SMPS**

DM Source Impedance is the impedance between line and neutral as shown in Figure 4.2. The major components of DM noise source impedance are the turned-on resistance of rectifying diodes, the equivalent series resistance (ESR) and equivalent series inductance (ESL) of the bulk capacitor. Other factors, such as the PCB layout, component placement and wiring layout also influence the noise source impedance.

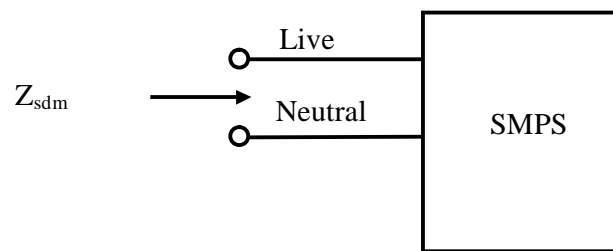


Figure 4.2 DM source impedance of SMPS

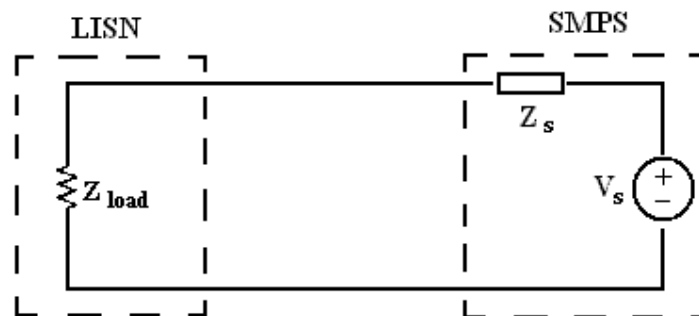


Figure 4.3 Simplified noise source circuit

**Chapter 4****Measurement of Noise Source Impedance of SMPS**

---

By following the above definitions, the noise source can then be reduced to a one-port Thevenin equivalent circuit as shown in Figure 4.3. Notice that in Figure 4.3,  $Z_s$  is  $Z_{scm}$  in the case of CM and  $Z_{sdm}$  in the case of DM.

Using the actual value of the noise source impedance obtained from a particular converter, its EMI filter topology and filter component values can be appropriately selected. Resonance between the noise source impedance and filter components can also be predicted based on the information. Furthermore, high frequency performance of a specific filter is also predictable provided the characteristics of the filter are known. However, there are several reasons, both theoretical and practical, why it is difficult to characterize the noise source impedance of SMPS. They are described in the following:

- The DM and CM conducted emissions are coupled through different paths to the point where conducted emissions are measured. Equipment package and component layout all affect the coupling paths, but the effects are very difficult to quantify. Often, a seemingly small change in layout could lead to significant change in the noise source impedances.
- Beyond a certain frequency, the effects of some high frequency parasitic elements start to surface. High frequency effects include permeability reduction of choke core, parasitic capacitance effect of the inductor, and parasitic inductance effect of the capacitor.
- At high frequency, the radiation coupling between SMPS and the circuits in vicinity and the coupling between components of SMPS will also affect the noise source impedance.

Due to the complexity of the CM and DM noise coupling mechanism, complete theoretical models may not be easily derived. Hence, the best way to determine their characteristics is still through measurement, even though it can be quite a challenging task.

In SMPS's operation, its circuit topology is continuously changing due to the switching actions. The currents flow in different paths in each operation stage of the switching circuit. Therefore, the noise source impedance measurement has to be made when the SMPS is operating at its intended loading condition. So far, very limited research has been done on determining the noise source impedance of SMPS.

## **4.2 Measurement with the two Current Probes Method**

To overcome the problems faced by the previously mentioned methods, the two current probes method is adopted for the measurement of the SMPS's noise source impedance. Using one current probe as an injection probe and the other current probe as a receiving probe, CM and DM noise source impedances in the EMI regulated frequency range of any SMPS can be determined with ease. As mentioned in Chapter 3, with careful calibration of the measurement setup, good accuracy can be achieved for measuring both CM and DM noise source impedances.

### 4.2.1 Measurement of CM Mode Noise Source Impedance for SMPS

The measurement setup for the CM noise source impedance of a SMPS is shown in Figure 4.4. The two 1  $\mu$ F capacitors (one for live to ground and another for neutral to ground) together with the injecting current probe and receiving current probe form the CM coupling circuit to avoid direct connection to the power mains. To isolate the LISN from the coupling circuit, a CM choke is inserted between the LISN and the SMPS during the measurement. The CM choke provides sufficient isolation between the LISN and SMPS in the interested frequency range (from 150 kHz to 30MHz), but does not affect the 50Hz/60Hz ac power. Normal power line CM choke is able to fit this purpose.

If the CM chock provides sufficiently large CM impedance at the measurement frequencies, the measurement setup shown in Figure 4.4 can be simplified to the equivalent circuit shown in Figure 3.3. With the expressions derived in Chapter 3, the CM noise source impedance of the SMPS can be obtained with the injected signal level and received signal level at the measurement frequencies. By conducting the measurement at a series of frequencies in the frequency range interested, the characteristics of the CM noise source impedance over the frequency range of interest can be determined.

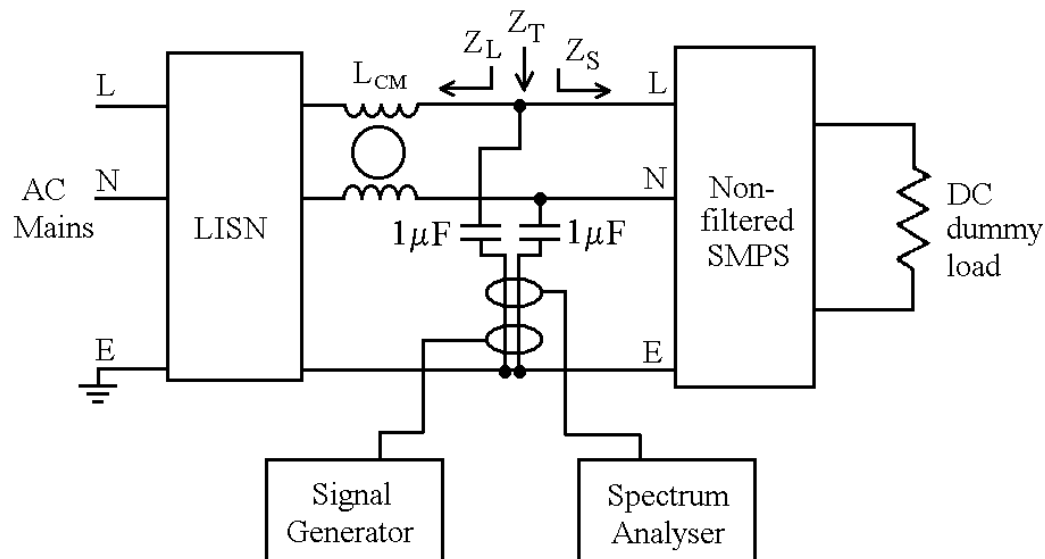


Figure 4.4 Measurement setup of SMPS's CM noise source impedance

### 4.2.2 Measurement of DM Noise Source Impedance for SMPS

Figure 4.5 shows the test setup for the DM noise source impedance measurement of SMPS. For ease of changing CM setup to DM setup, the two  $1\mu F$  capacitors used in the CM setup will still be employed in the DM setup. Now, the two coupling capacitors are in parallel and connected between live and neutral. Again to isolate the effect of the LISN and ac main lines in high frequency, two DM chokes are added between the LISN and the SMPS. Same as the measurement of CM noise source impedance measurement, if the DM chokes provide sufficiently large DM impedance



## Chapter 4

## Measurement of Noise Source Impedance of SMPS

at the measurement frequencies, a condition which is very easy to meet by using two DM chocks effective in the required frequency range, the measurement setup shown in Figure 4.5 can be simplified to the equivalent circuit shown in Figure 3.3. Based on the procedures derived in Chapter 3, the DM noise source impedance of the SMPS can be obtained with the injected signal level and received signal level at the measurement frequencies. The measurement is also made at a series of frequency in the interested frequency range.

As the objective of this measurement is to obtain the noise source impedance for EMI filter design purposes, the SMPS under measurement is a non-filtered SMPS. The EMI filter for the non-filtered SMPS will be designed based on its impedance characteristics obtained in the measurement. During the measurement, the SMPS is operating in its normal operation conditions with its typical load. Hence, the measured impedance reflects the true impedance of the SMPS in its intended operating condition.

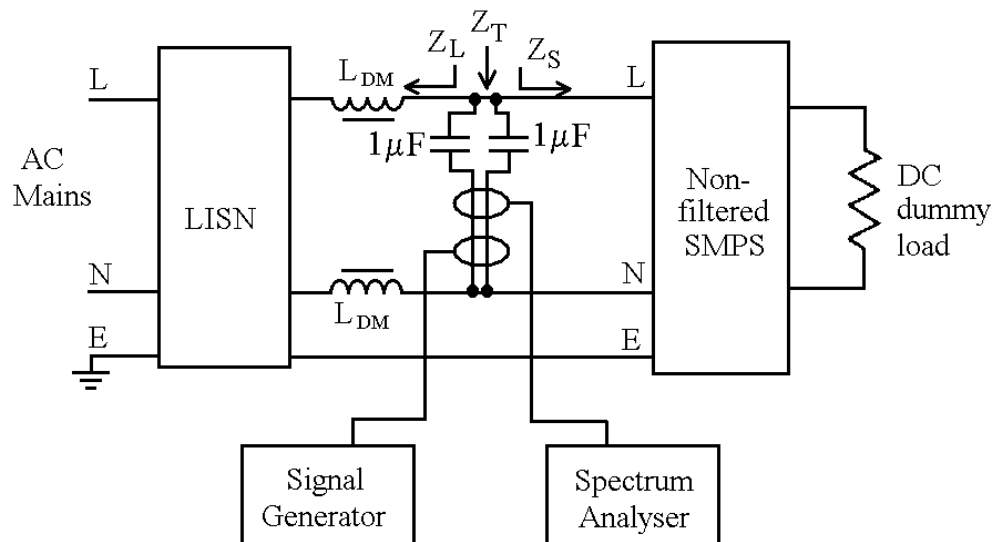


Figure 4.5 Measurement setup of SMPS's DM noise source impedance

### 4.3 Experiment Results

Same as the measurement setup proposed in Chapter 3, a Tektronic CT-1 current probe (5mV/mA, bandwidth 25 kHz to 1000 MHz) and a CT-2 current probe (1mV/mA, bandwidth 1.2 kHz to 700 MHz) are chosen as the injecting current probe and receiving current probe, respectively. The HP 8591E spectrum analyzer with an internal tracking signal generator module is employed for the measurement. The data acquisition was performed with “HP Benchlink” software at an IBM notebook PC connected to the spectrum analyzer with GPIB cable. In both CM and DM noise source impedance measurement setups shown above, the RF coupling circuit consists of two 1  $\mu$ F capacitors, the injecting current probe and the receiving current probe. To ensure  $Z_{setup}$  of the RF coupling circuit is repeatable, the two capacitors are mounted on a printed circuit board (PCB) and two fixed positions have been marked on the PCB for the injecting probe and receiving probe. Also, the final wire connections from the PCB to the points of measurement have been made as short as possible to minimize the parasitic effect due to wire positioning. The actual implementation of the RF coupling circuit is shown in Figure 4.6. The advantage of fixing the coupling circuit for both setups is that once it is calibrated to obtain  $Z_{setup}$ , it can be used for both CM and DM setups to speed up the noise source impedance measurement process. The measured  $Z_{setup}$  of the RF coupling circuit is plotted in both Figure 4.7 and Figure 4.8. By observing the change in measured magnitude of  $Z_{setup}$  with respect to frequency,

it can be modeled as a resistor of  $1.12\ \Omega$ , an inductor of  $240\ \text{nH}$  and a capacitor of  $2.05\ \mu\text{F}$  in series.

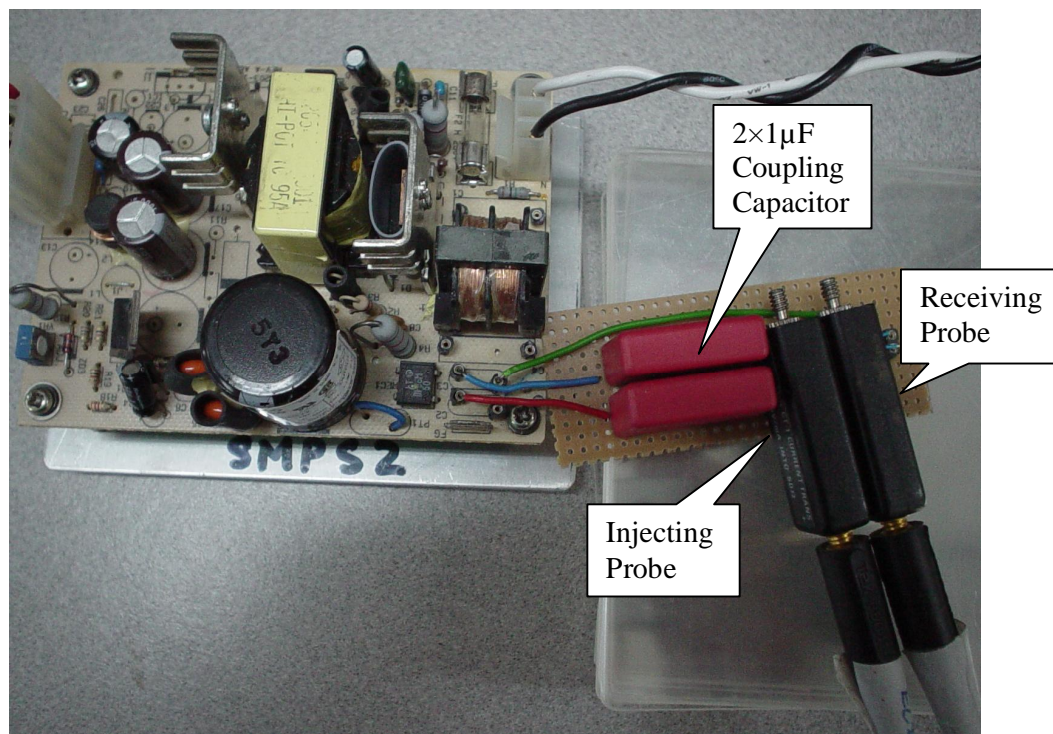


Figure 4.6 Implementation of the RF coupling circuit

Figure 4.9 shows the measured impedance magnitude of  $Z_{\text{setup}}$  with that obtained from the series  $RLC$  equivalent circuit model ( $R = 1.12\ \Omega$ ,  $L = 240\ \text{nH}$  and  $C = 2.05\ \mu\text{F}$ ). It shows that in the frequency range of interest ( $150\ \text{kHz} - 30\ \text{MHz}$ ), the proposed equivalent circuit model is adequate to represent  $Z_{\text{setup}}$ .

## Chapter 4

## Measurement of Noise Source Impedance of SMPS

The actual measured impedance of the RF coupling circuit is  $Z_T$ , which is  $Z_L$  and  $Z_s$  in parallel, where  $Z_s$  is the actual noise source impedance to be measured and  $Z_L$  is the RF isolation to be provided by suitable chokes. If sufficient RF isolation is provided and  $Z_L \gg Z_s$ , then  $Z_T \approx Z_s$ . For the CM setup, a 16 mH CM choke (Coilcraft CMT3-16-2) is inserted between the LISN and the SMPS to provide CM RF isolation. For the DM setup, two 350  $\mu$ H DM chokes (Zion VSM 300) are added between the LISN and the SMPS to provide the DM RF isolation.

A SMPS (ASTECH RBS22, 22W, 230 V/0.5 A) is used as an example to illustrate the steps to obtain the CM and DM noise source impedances. The rated currents for the selected CM and DM chokes are 2 A and 3 A, respectively. Since the rated current of the SMPS is much lower than the current ratings of the chokes, we do not expect core saturation to happen for the chokes. First the SMPS is removed from the ac mains and the coupling circuit measures essentially  $Z_L$  only. Then the SMPS is connected back to the ac mains and now the coupling circuit measures  $Z_T$ .

Figure 4.7 shows the measured  $Z_L$ ,  $Z_T$  and  $Z_{setup}$  in the frequency range of 10 kHz to 30 MHz for the CM setup. From 10 kHz to 40 kHz,  $Z_T \approx Z_L$ , it shows that  $Z_s \gg Z_L$ . It also indicates that the CM choke is not saturated, otherwise,  $Z_T \ll Z_L$ . Above 40 kHz, the CM choke begins to provide good RF isolation. Since  $Z_{setup}$  is very small as compared to  $Z_T$ ,  $Z_T \approx Z_s$ . A series resonance at approximately 8 MHz is observed because the capacitive reactance of  $Z_s$  is equal to the inductive reactance of  $Z_{setup}$ . Above 8 MHz, the measured impedance is dominant by  $Z_{setup}$  and  $Z_s$  cannot be determined. Based on the trend of  $Z_T$  with frequency between 40 kHz to about 8 MHz, it is quite obvious that  $Z_s$  is capacitive in nature with a capacitance of 950 pF.

## Chapter 4

## Measurement of Noise Source Impedance of SMPS

Figure 4.8 shows the DM measurement results from 10 kHz to 30 MHz. For the full frequency range,  $Z_T \ll Z_L$ , it shows that the DM chokes provide good RF isolation for the entire frequency range. Since  $Z_T$  is now comparable to  $Z_{setup}$ , the effect of  $Z_{setup}$  cannot be ignored and the DM noise source impedance must be determined by  $Z_s = Z_T - Z_{setup}$ . Based on the trend of magnitude change of  $Z_T$  with frequency,  $Z_T$  can be modeled by a series  $RLC$  circuit with  $R = 2.7 \Omega$ ,  $L = 320 \text{ nH}$  and  $C = 2.05 \mu\text{F}$ . Figure 4.10 shows the measured  $Z_T$  and the calculated  $Z_T$  from the proposed equivalent circuit model. It shows that in the frequency range of interest, the proposed equivalent circuit can be used to represent  $Z_T$  with good accuracy. With known circuit model of  $Z_{setup}$  (series  $RLC$  with  $R = 1.12 \Omega$ ,  $L = 240 \text{ nH}$  and  $C = 2.05 \mu\text{F}$ ), we can obtain  $Z_s$  by subtracting  $Z_{setup}$  from  $Z_T$ , which can be represented by series  $RL$  circuit with  $R = 1.58 \Omega$  and  $L = 80 \text{ nH}$ . Hence, for the frequency of interest, if the impedance changes with frequency is either  $+ 20 \text{ dB/decade}$  or  $- 20 \text{ dB/decade}$ , we only need the magnitude information of the measured impedance to extract the equivalent circuit model with good accuracy.

As the two-current-probe setup allow measurement of the noise source impedance of the SMPS under the normal “power on” condition, it has the flexibility to determine the noise source impedance of the SMPS for different loading conditions. The merit of the two-current-probe setup is its pre-measurement calibration process for the RF coupling circuit. With this calibration process, the impedance due to the RF coupling circuit,  $Z_{setup}$ , can be measured and accounted for. Hence, possible error contributed by the RF coupling circuit can be eliminated to achieve good accuracy for the measurement of noise source impedance of the SMPS.

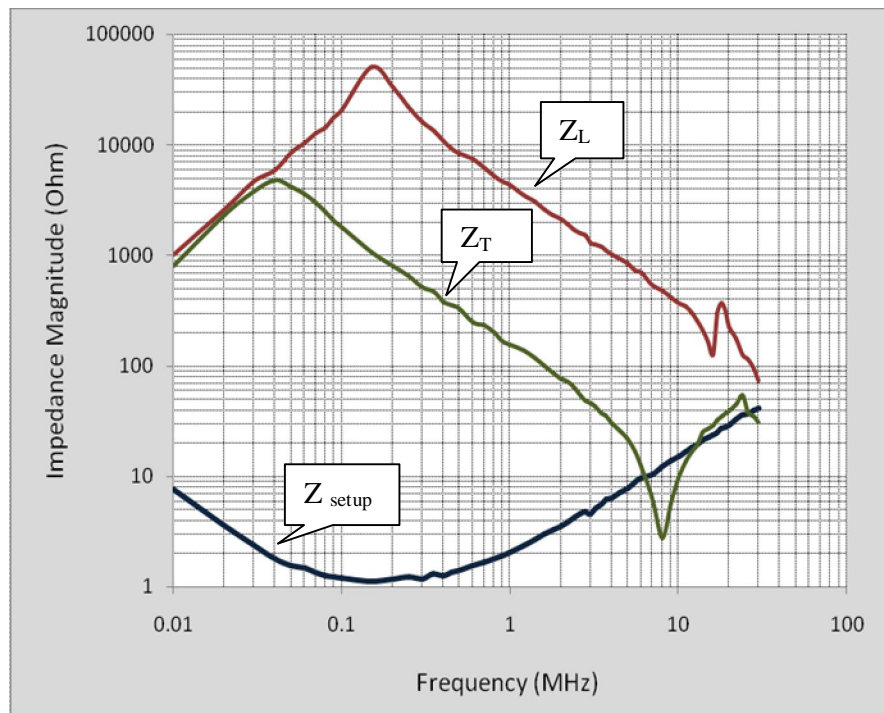


Figure 4.7 CM noise source impedance measurement

The CM noise source impedance is usually capacitive in nature. It resonates with the inductive element of the RF coupling circuit at some frequency below 30 MHz, which imposes the maximum frequency limit for the CM noise source impedance measurement. The resonant frequency can be pushed up further by reducing the inductive element of the RF coupling circuit, which can be achieved by selecting a coupling capacitor with a lower ESL and making the RF coupling circuit more compact. Also, for SMPS with high power rating, special attention must be paid to ensure that the CM and DM chokes are not saturated while providing the necessary RF

isolation. This can usually be resolved by putting two chokes of lower inductances and higher current ratings in series.

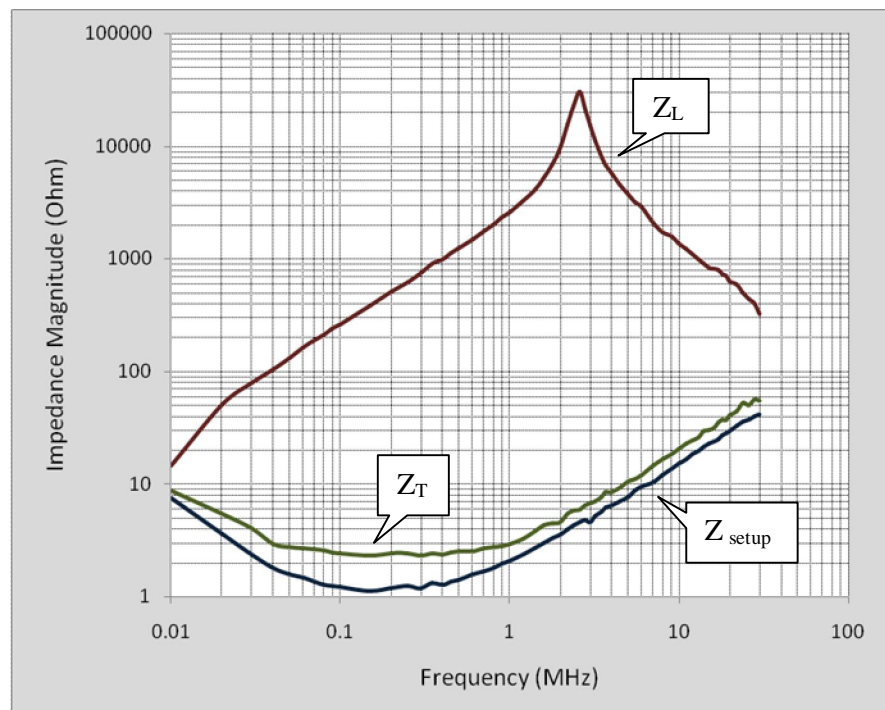


Figure 4.8 DM noise source impedance measurement



## Chapter 4

## Measurement of Noise Source Impedance of SMPS

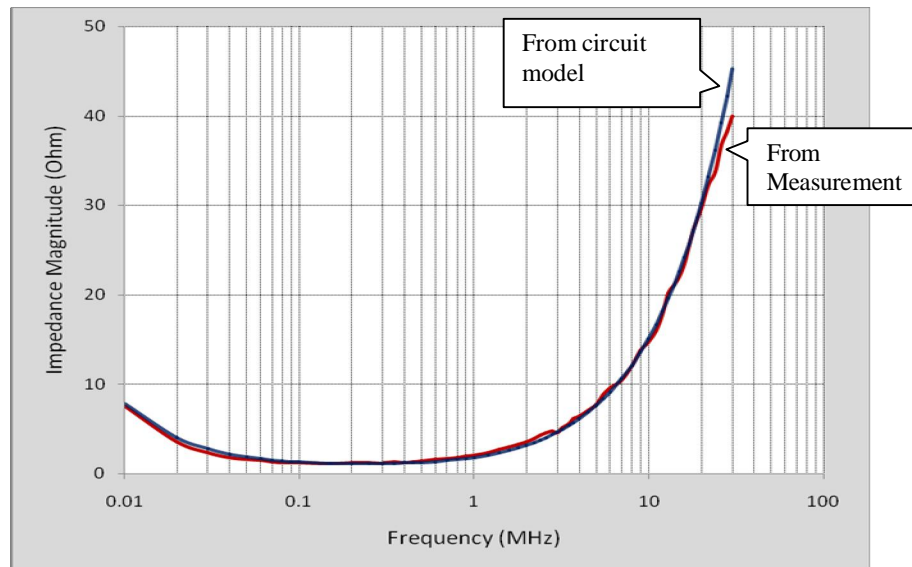


Figure 4.9 Comparison of the measured and calculated  $Z_{setup}$

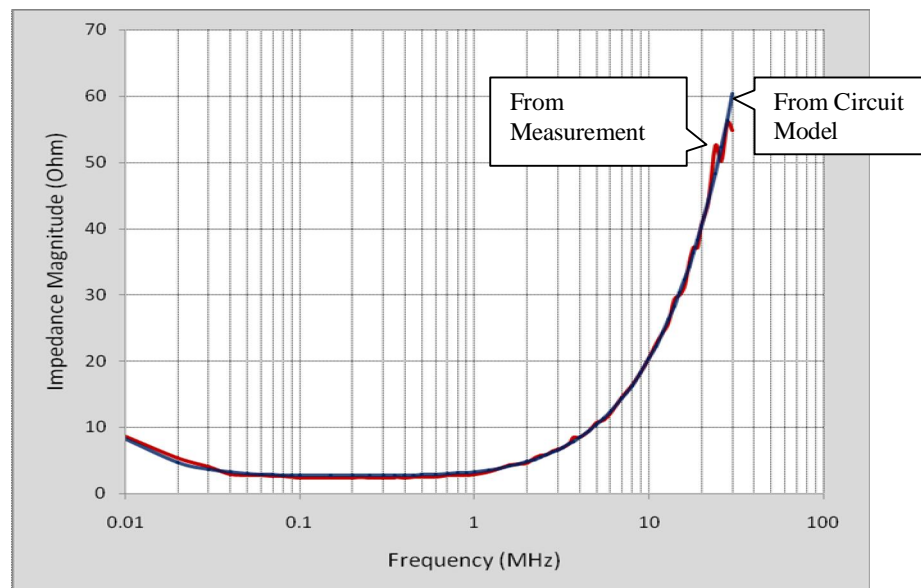


Figure 4.10 Comparison of the measured and calculated  $Z_T$



## Chapter 5 Characterization of EMI Chokes

### 5.1 EMI Filter Components

Typically, an EMI power-line filter consists of shunt capacitors and series inductors. The components of an ac power line EMI filter are subject to two important requirements: they must safely tolerate the nominal operating voltage and current of the electrical equipment, and their high frequency characteristics must not vary with frequency. However, EMI filter components are usually non-ideal within the frequency reduction band of EMI. In the frequency range of 150 kHz to 30 MHz, the equivalent circuit of EMI components becomes a two-terminal network containing several components. The characteristics of EMI components in reality varies significantly with frequency, which makes the performance of EMI filter deviates from the expectation. The characterization of EMI filter components is crucial for conducted emissions suppression design.

Real capacitors are not purely capacitive, even at low frequency, since their leakage resistance of the isolation  $R_p$  and equivalent series resistance (ESR)  $R_s$  cannot be neglected in every case. At higher frequencies, the effect of the stray inductances  $L$  is also considerable. For dc current, the impedance of a real capacitor equal to its leakage resistance  $R_p$ . With increasing frequency, the reactance of this capacitor will

be lower than its leakage resistance  $R_p$ . With a further increase in frequency, the impedance of the real capacitor will be determined more and more by its parasitic inductance  $L$  instead of its capacitance. This means that the real capacitor behaves more like an inductor than a capacitor at high frequency. The capacitor will resonate at its self-resonant frequency  $\omega_o$ . A real capacitor can be regarded as capacitance only in the frequency range below its self-resonant frequency. The impedance of the capacitor is just  $R_s$  (ESR) at its self-resonant frequency. At frequencies higher than its self-resonant frequency, the capacitor behaves like an inductor and is, therefore, no longer effective as an EMI power-line filter component.

In engineering practice, the high frequency characteristics of real EMI filter capacitors are examined by means of equivalent circuit with an ideal capacitor  $C$ , an equivalent series resistance  $R_s$  and an ideal inductor  $L$  connected in series. The effect of the leakage resistance  $R_p$  is negligible in the analysis. The serial parasitic inductance is principally the result of three partial inductances: the inductance of the wound structure,  $L_s$ , the inductance of internal leads,  $L_l$ , and the inductance of the connecting wires  $L_w$ . The value of  $L_s$  and  $L_l$  depends on their dimensions and structure of the capacitor. This inductance is generally about 5 to 50nH. The inductance of connecting leads,  $L_w$ , is related to the length and diameter of the connecting wires. EMI filter capacitors can be well characterized by the resonance frequency  $\omega_o$ . To increase the effective frequency range where the real capacitor acts like a capacitance, noise suppression capacitor with the highest possible resonance frequency should be applied. Therefore, only capacitors with low parasitic inductance are suitable for EMI filter. In practice, for a selected EMI filter capacitor, the internal parasitic inductances  $L_s$  and  $L_l$  cannot be changed, and the connecting wires are usually the major factors of

inductance that determine the resonant frequency. Therefore, connecting wire length should be kept to an absolute minimum for noise suppression.

The impacts of applied voltage and loading current on the characteristics of EMI filter capacitor are not significant. The capacitor can be well characterized with off-the-shelf equipment like RF impedance analyzer, network analyzer, RLC meters etc. under no load conditions. Normally, EMI filter designers can rely on the parameters and characteristics of EMI filter capacitors provided in the manufacturer's catalogues or data sheet in their work.

Real inductors are not purely inductive. The windings by their very nature will be shunted by distributed capacitance. Therefore, inductors too suffer from self-resonant characteristics. Above their self-resonant frequency, the capacitance dominates so that inductors lose their effectiveness at higher frequencies. Depending on the value of the inductance, the geometry of the windings, and the core material, coil self-resonance typically may occur in the range of 150 kHz to 2 MHz.

It is quite clear that the design of inductors must take into account the saturation characteristics of the core material due to the current rating of the filter and the turns required. Otherwise, the core would be saturated under normal operating conditions and would be ineffective as a filter component. An identical inductor cannot be expected to perform identically or similarly in two different applications due to the differences in the load current (amplitude, waveform, frequency, etc.) as well as some parasitic phenomena. The parameters and characteristics of EMI filter inductors provided in the manufacturer's catalogues or data sheet can only be taken as a reference. The performance of the EMI filter inductors in an actual application still depends greatly on the measurement under their actual operation conditions.

## 5.2 EMI Chokes

EMI filter inductors may come with two forms. The most common form is a single magnetic core structure wound with two coupled windings, one connected in the line conductor and the other in the neutral conductor. This type of inductor is also called as CM choke because it is mainly used to suppress the CM noise. In the other form, independent and single-winding inductors are used in either or both lines. Only DM noise can be suppressed with this type of inductor, therefore, it is also called as DM choke. In the case of multiphase or split-phase filters, the CM choke have identical windings, one for each power-carrying line. Similarly, the DM choke would appear in each of these lines. For clarity, principles will be discussed with reference to single-phase filters in this thesis.

### 5.2.1 CM Choke

High CM inductance is often required to suppress CM noise as value of Y capacitor is restricted in the nF range due to the electrical safety consideration. The goal of creating a choke coil that displays high impedance for CM noise components but low impedance against DM noise components can be accomplished with the development of CM choke. The CM choke consists of identical windings placed on a

closed ferrite core. Figure 5.1 shows the structure of a CM choke. The two windings of such a component are designed with an equal number of turns so that the magnetomotive force around the core due to the power frequency current in these windings cancels each other. In the figure, it can be seen that the net magnetomotive force around the core is zero because of the cancellation of the ampere-turns ( $NI$ ) associated with each winding. Therefore, if one stops at this point, one will conclude that such a coil structure will never saturate. This is not the case, however, because of leakage flux, which is not coupled from one winding to another. These independent fluxes can cause the core material to saturate in the regions where they exist. This saturation, even though it is localized, will have the same effect as the introduction of a large air gap in the core. That is, the inductance of the windings will decrease dramatically.

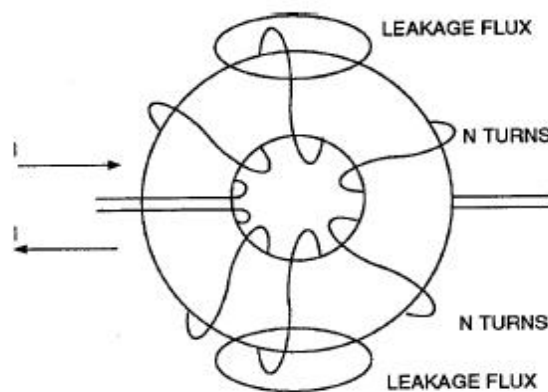


Figure 5.1 Structure of CM EMI choke

As the most of mains frequency magnetomotive forces around the core are cancelled each other, the core may be of high magnetic permeability, allowing a large CM inductance with only a few turns. The relative permeability of ferrite cores decreases with an increase in frequency; thus, the inductance of the CM choke also changes as a function of frequency. The inductance of CM choke coils decreases at gyro-magnetic frequency to about the half of initial value. The gyro-magnetic frequency of ferrite cores is in the megahertz order.

In case of perfect compensation of the mains frequency magnetizing force in the ferrite core, the inductance of common mode choke coils might not depend on mains frequency currents, but perfection is not always achieved in practice. In actual application, this imperfect compensation is used to suppress DM EMI noise. The impedance of the CM choke for DM noise is proportional to the leakage between the two coils of the choke, a result of imperfect compensation of DM components. Therefore, the leakage inductance of the CM choke coil can be used to suppress DM conducted emissions. In many industry applications, no separate DM choke coil can be found in the EMI filter circuit, the circuit designer use the CM inductance of the CM choke coil as the inductor of the CM EMI filter circuit and the leakage inductance of the CM choke coil as the inductor of the DM EMI filter circuit. The leakage impedance of CM choke coil is also called as DM impedance of CM choke coil.

Saturation is a very important consideration in the design of CM Choke coils. The ferrite core may saturate due to the imperfect compensation of mains frequency magnetizing force, which resulting in drastically decreasing of common mode inductance of the choke.

### 5.2.2 DM Choke

The DM choke for EMI filtering are usually single-layer solenoid structure. The scheme of a solenoid-type choke coil is shown in Figure 5.2. Suitable formulas are known for calculating the inductance of such coil arrangements, if the internal and external diameters are not very different, and if the coil length is much higher than its diameter (i.e. length  $> 0.3D$ ) [3]:

$$L = \frac{(\pi ND)^2}{l + 0.45 \times D} \times 10^{-7} \text{ H} \quad (5-1)$$

Where

$N$  = number of turns

$D$  = internal diameter of the coil in meters

$l$  = axial length of the coil in meters

In the case of multi-layer coils or choke coils made from a strip (flat) conductor of large cross-section, the internal and external diameter may become mutually commensurable. For calculating the inductance of such coils, substitute the average coil diameter in place of the diameter  $D$ , in equation (5-1). For reducing the stray capacitance between the turns, often some space is left between the turns of solenoid-type choke coils, i.e. the pitch of windings (denoted as  $p$  in Figure 5.2) is higher than the width of the conductor (denoted as  $d$  in Figure 5.2).

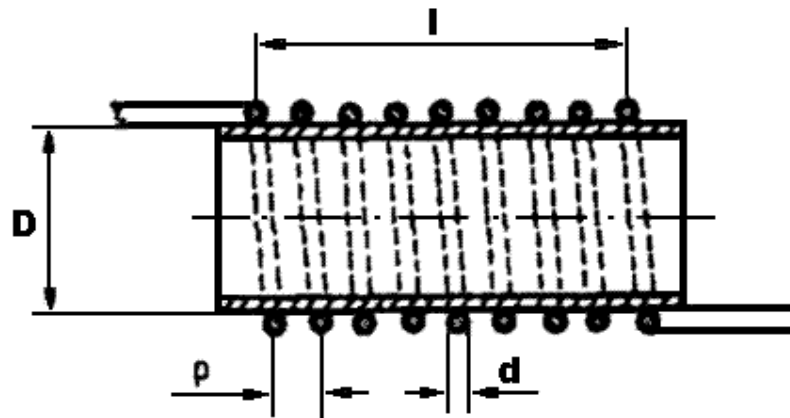


Figure 5.2 Structure of DM single-layer solenoid choke

### 5.2.3 Equivalent Circuit of EMI Chokes

Noise suppression choke can be well characterized in a wide frequency range by the equivalent circuit seen in Figure 5.3 which is necessary to understand the terms that define the performance and the limitation of inductors in the frequency range of conducted emissions suppression. The resistance in the equivalent circuit represents the losses of the choke. The parasitic effects at higher frequencies, resulting from the stray capacitances between turns, cannot be neglected in the analysis of the inductor's performance. Although the turn-capacitance is distributed, a parallel connected



concentrated capacitor provides a suitable approximation. The impedance of the choke according to the equivalent circuit is:

$$Z_L = \frac{R + j\omega L}{1 - \omega^2 LC + j\omega RC} \quad (5-2)$$

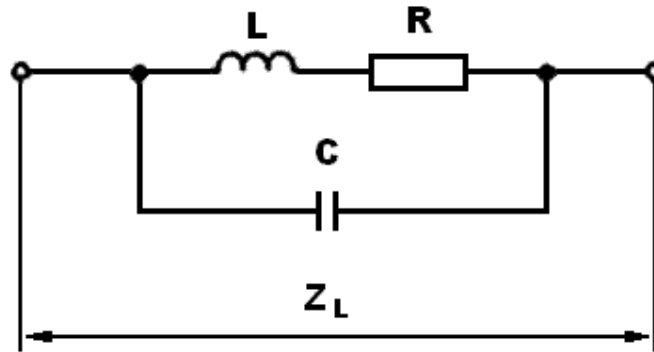


Figure 5.3 Equivalent circuit of an EMI choke

At low frequencies, impedance  $Z_L$  is dominated by inductance, and at dc it will be equal to  $R$ . In the frequency range of  $\omega_L$ , the impedance of the choke increases proportionally with frequency, as can be seen in Figure 5.4. At frequency  $\omega_o$ , the inductor,  $L$ , resonates with the parallel capacitor,  $C$ , and the impedance,  $Z_L$ , reaches its maximum. The maximum value increases with increasing  $Q$ -factor and decreasing series resistance. The impedance of the choke at low frequencies (more precisely, in the frequency range below the resonance angular frequency) with fair approximation is:

$$Z_L \approx R + j\omega L \quad (5-3)$$

At higher frequencies, the impedance of the choke decreases because the parallel capacitor dominates; i.e., the inductor acts like a capacitor. In this frequency range, the impedance of the choke with good approximation is as follows:

$$Z_L \approx \frac{j\omega L}{-\omega^2 LC} = \frac{1}{j\omega C} \quad (5-4)$$

The self-resonance angular frequency of the choke:

$$\omega_o = \frac{1}{\sqrt{LC}} \quad (5-5)$$

The  $Q$ -factor of the choke:

$$Q = \frac{\omega L}{R} \quad (5-6)$$

The impedance of the choke at resonance can be determined by means of equation (5-2) and (5-5). Supposing that the impedance of the choke at resonance is much higher than the series resistance, the impedance of the choke at resonance is:

$$Z_L(f_o) \approx \frac{L}{RC} \quad (5-7)$$

Using equations (5-5) and (5-6), we can get  $Q^2$  at  $\omega_o$ :

$$Q^2 = \frac{\omega_o^2 L^2}{R^2}$$

$$Q^2 = \frac{\frac{1}{LC} L^2}{R^2}$$

$$Q^2 = \frac{L}{R^2 C} \quad (5-8)$$

With equation (5-8), the impedance of the choke at resonance can be rewritten into the following form:

$$Z_L(f_o) \approx R \times Q^2 \quad (5-9)$$

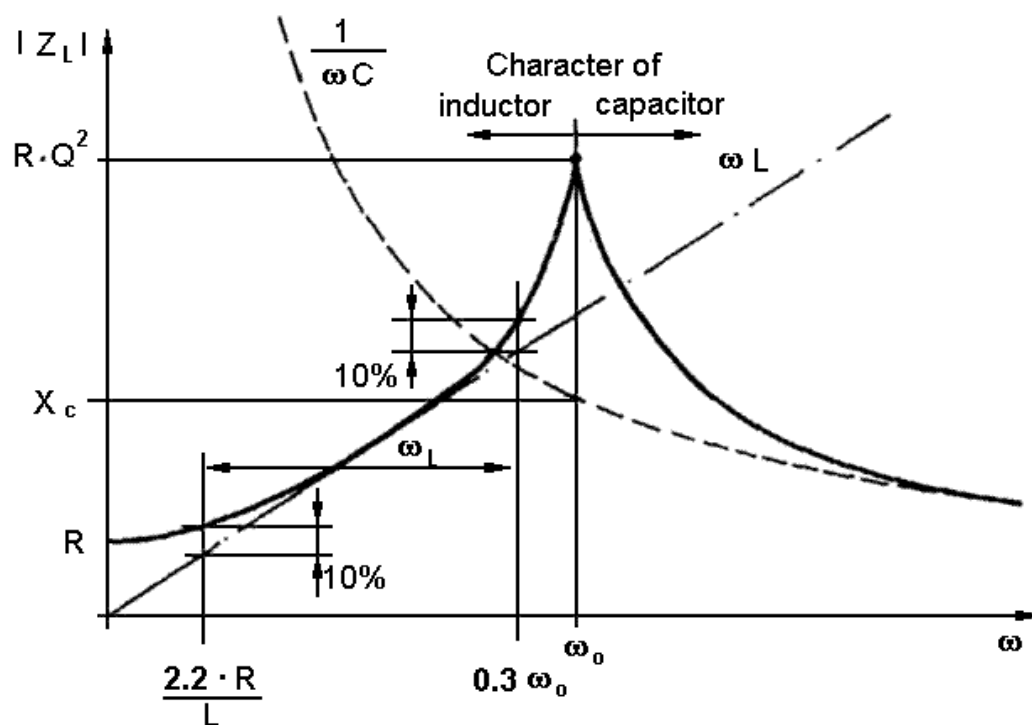


Figure 5.4 Impedance versus frequency of an EMI choke

### 5.3 In-Circuit Characterization of EMI Chokes

The effectiveness of a power line EMI filter in SMPS depends to a great extent on the characteristics of CM choke and DM choke under actual loading condition. The different material properties and construction of the chokes, in addition to their existing parasitic parameters, will cause two apparently identical chokes to behave differently in a given application. For CM and DM chokes used in EMI filter of SMPS, besides the magnetic material saturation, core loss and some other parasitic effects, the varying CM noise source impedance and DM noise source impedance of the operating SMPS will also cause the CM and DM chokes to perform differently from the technical specifications provided by their manufacturers. Therefore, the measurements of CM choke and DM choke impedance under different loading condition, especially in its actual application configuration, are important in estimating the actual filter attenuation of the designed power line EMI filter.

The proposed two-current-probe method described in Chapter 3 can be extended to measure the impedance of either CM or DM EMI choke, under the actual loading conditions. Using one current probe as an injecting probe and the other current probe as a receiving probe, the CM and DM impedances of EMI chokes in the conducted EMI regulated frequency range (normally 150 kHz – 30 MHz) can be determined accurately under actual current loading.

### 5.3.1 Measurement of CM impedance of CM choke

CM chokes are crucial components in the power line EMI filters for power conversion product such as SMPS and uninterruptible power supplies (UPS). With the proposed two-current-probe measurement approach, it is possible to measure the impedance of a CM choke under in-circuit operating condition. By varying the load current, the CM impedance behavior of the choke can be easily observed. Figure 5.5 shows the measurement setup to characterize the CM impedance of the CM choke. The circuit where the CM choke is inserted resembles that of a typical SMPS. The DM load circuit consists of a bridge rectifier, a bulk capacitor  $C_d$  and a load resistor  $R_d$ . The load also can be an actual SMPS or any kinds of application circuit in front of which the CM choke will be installed. That means the measurement can be made in the actual application circuit so that the characteristics of choke in the actual applications can be obtained with this method. By connecting the DM load circuit to a programmable ac power source, repetitive dc current pulses are generated so that it emulates the actual operating condition where the CM choke is supposed to work. The magnitude of the DM current pulse can be varied with the programmable ac power supply.

The two 1  $\mu$ F capacitors (one between live-to-ground and another between neutral-to-ground) and the injecting current probe and receiving current probe form the CM coupling circuit for the CM choke-under-test. In order to complete the CM signal path, two 2200 pF capacitors (one between live-to-ground and another between neutral-to-ground) are added on the other end of the CM choke. The value of 2200 pF is chosen

because this is the typical value commonly used in SMPS or UPS for EMI filtering purposes. The RF signal is injected into the CM signal path through the injecting current probe, which is connected to the output port of a signal generator. The resulting RF signal in the CM signal path is measured by RF input port of a spectrum analyzer via the receiving current probe. The CM impedance of the CM choke-under-test can be obtained using the procedures described in the Chapter 3. To ensure the impedance of the measurement setup of the CM signal path,  $Z_{setup}$ , is stable and repeatable, all the capacitors are mounted on a PCB. Also, two fixed positions on the PCB are labeled for the placements of the injecting current probe and receiving current probe. The wire connections on the PCB have been made as short as possible to minimize the loop inductance of the coupling circuit. Firstly, without the CM choke-under-test, the CM impedance of the measurement setup ( $Z_{setup}$ ) is measured. Then, the CM choke-under-test is inserted and the CM impedance is measured again. If the effect of  $Z_{setup}$  cannot be ignored, it should be subtracted from the second set of measurement.

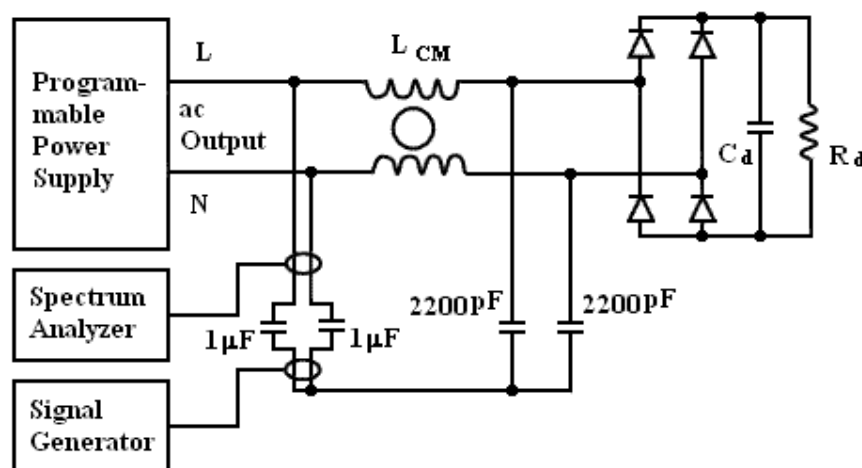


Figure 5.5 Measurement setup to characterize CM impedance of a CM choke

### 5.3.2 Measurement of DM Impedance of CM Choke

The DM impedance of CM choke is due to the imperfect cancellation of magnetizing force in the core due to the DM noise current. This DM impedance can be doubled up as a DM inductor in suppressing DM noise generated in the circuit. The impedance of the DM choke is independent of the load current if the load current is well below the saturation current of the choke. However, when the load current is approaching to the saturation current point, the DM impedance will drastically decrease to a very small value, especially in the vicinity of its self-resonant frequency, mainly due to the core losses such as hysteresis losses and eddy current losses. The other factors which affect the DM choke's impedance value are resistive loss, dielectric losses and temperature rise.

Similarly, with the two-current-probe, the DM impedance of a CM choke under loading conditions can be measured over a wide frequency range. Figure 5.6 shows the principle of the DM impedance measurement setup for a CM choke. It is recommended to use the same RF coupling circuit that used in the CM impedance measurement in order to eliminating the double work in the system calibration and measurement of  $Z_{setup}$ . The load which consists of a bridge rectifier B, a bulk capacitor  $C_d$  and a load  $R_d$  can also be replaced by an actual application circuit such as a SMPS, UPS, etc. The 2 inductors  $L_B$ s are used to eliminating the effects from the variable ac source and the load circuit. The total inductance of the two  $L_B$  should be much greater than that of the  $L_{DM}$  ( $2 \times L_B \gg L_{DM}$ ) in order to fit the isolation purpose. The  $L_B$

should not be saturated throughout the measurement. Same as the CM impedance measurement, the amplitude of load current can be adjusted by changing the amplitude of the input ac voltage.

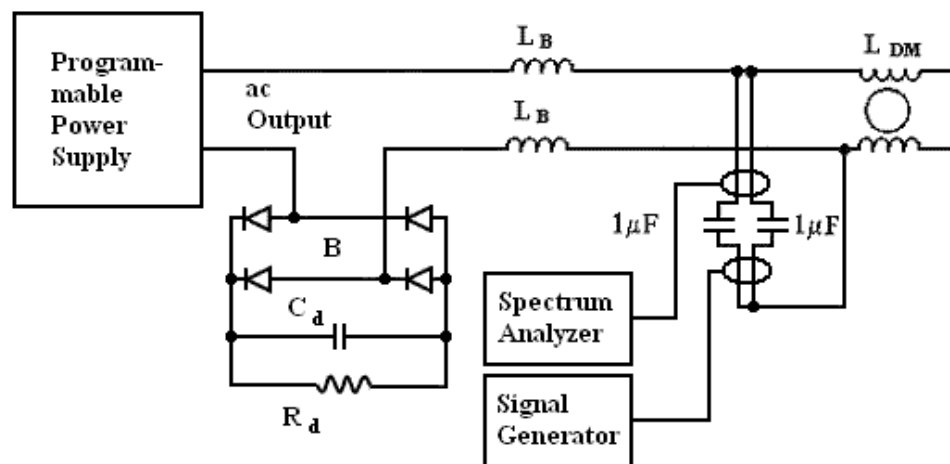


Figure 5.6 Measurement setup to characterize DM impedance of a CM choke



### 5.3.3 Impedance Measurement for DM Choke

The same principle can be applied in the impedance measurement of normal choke which is quite often used as DM choke in EMI filter circuit. Figure 5.7 shows the two-current-probe measurement setup with a load circuit consist of a bridge rectifier  $B$ , a bulk capacitor  $C_d$  and a load resistor  $R_d$ . Same as the measurement of CM choke impedance, the load circuit can be an actual application circuit, and the function of the two  $L_B$  is to eliminate the effect of the ac source and the load circuit in the impedance measurement. The amplitude of load current can be adjusted by changing the amplitude of the input ac voltage. The procedures to conduct the measurement are also the same.

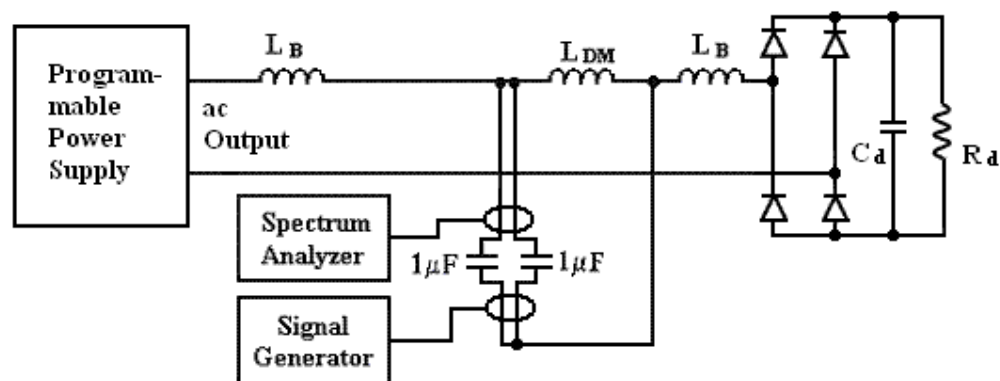


Figure 5.7 Measurement setup to characterize DM choke

## 5.4 Experiment Results

The measurement setup in the laboratory is shown in Figure 5.8. Again, Tektronic CT-1 current probe and CT-2 current probe are chosen as the injecting probe and receiving probe, respectively. A HP Spectrum Analyzer HP 8593E is employed for the measurement of the RF signal received via the receiving probe, while, the injected RF signal came from the output port of the tracking signal generator module inside the spectrum analyzer. The readings of the spectrum analyzer over the whole frequency range of interest were captured to a notebook PC in a few seconds with a data acquisition software “HP Benchlink” via a GPIB connection between the PC and the spectrum analyzer. A pre-amplifier is used in the signal path as the signals are very weak when the RF impedance is great. The ac source used in the measurement is an ELGAR SW 5250A programmable power supply. A CM choke, model: Tokin SS24V-R15080, is chosen for evaluation. The load circuit consists of a bridge rectifier, a 220  $\mu$ F electrolytic capacitor and a 100 $\Omega$  aluminum wire-wound resistor with a maximum power rating of 300W, which is used to simulate a SMPS. The loading current of the CM choke is adjusted by changing the output voltage amplitude of the programmable power supply during the measurement. As before, the CM coupling circuit is calibrated with a standard known resistor and followed by characterization of the measurement setup. Then, the CM choke is added to the measurement setup as shown in Figure 5.5. The Figure 5.8 shows the actual implementation of Figure 5.5 in the laboratory.

Figure 5.9 shows the CM choke, RF coupling circuit including the two-current-probe, and the load circuit built in the laboratory. The CM impedance of the choke is measured in the frequency range from 50 kHz to 10 MHz. In the frequency range of interest, the impedance of the measurement setup,  $Z_{setup}$ , is much smaller than the CM impedance of the choke, as shown clearly in Figure 5.10. Figure 5.11 shows the measured CM impedance of the choke under varying load current condition. When the peak magnitude of the current pulse is less than 5.21A, the CM choke provides excellent CM impedance, with at least 1k $\Omega$  up to 5 MHz. As usual, a self-resonate frequency at 353 kHz is observed. If the peak current is higher than 5.21A, the CM impedance of the choke begins to decrease as a sign of core saturation. This behavior is clearly observed in Figure 5.11. When the peak current increases to 6.11A, CM impedance at resonance has dropped from 24.5 k $\Omega$  to about 8.1 k $\Omega$ . Further increase in peak current, for examples, at 7.10A, the choke practically offers no CM impedance at all. Ideally, the AC mains current in the live and neutral lines is DM in nature and should not have any impact on the CM impedance of the CM choke. However, in reality, the magnetic fluxes in the ferrite core due to the windings for the live and neutral lines can never cancel totally. Hence, it results in finite flux in the ferrite core. Once the AC mains current increases further, it will reach a point when the resultant flux circulating in the core causes core-saturation. For the given CM choke, it shows that its CM attenuation performance is significantly reduce when the peak current goes beyond 5.21 A.

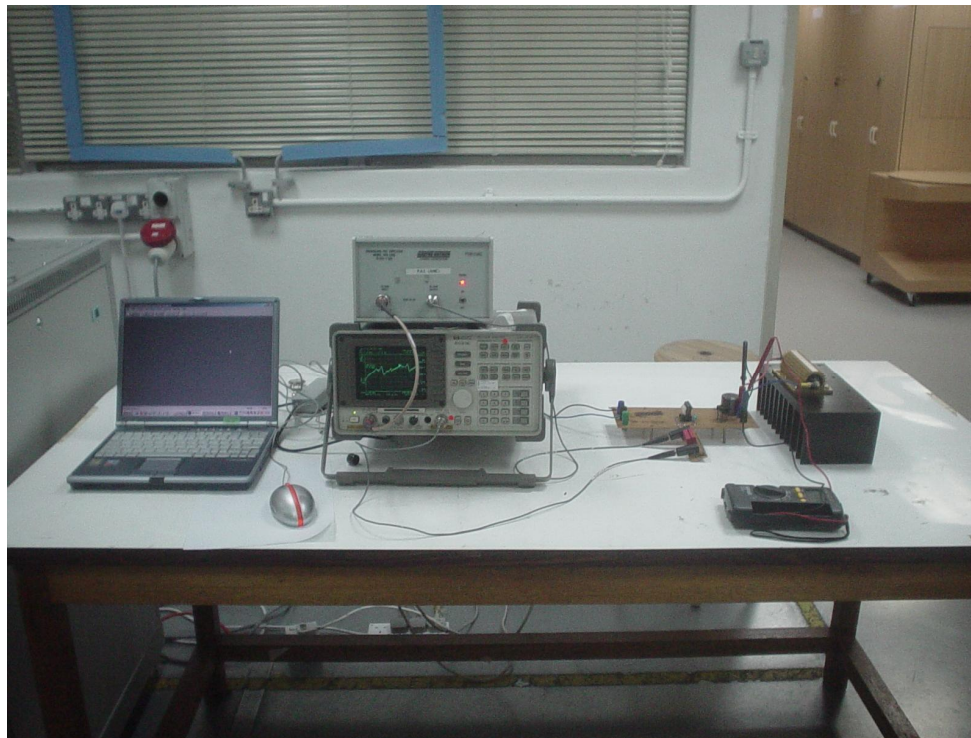


Figure 5.8 Measurement setup for characterization of chokes in lab

The impact of the core loss due to the load current is significant to the CM impedance in the vicinity of its self-resonate frequency. This impact is not significant to the CM impedance at higher frequency. In the vicinity of self-resonant frequency of the CM choke, the CM impedance is very high (around 25 k $\Omega$ ) when the current is below its rated current, and the amplitude of the signal received by the receiving probe

is very low. Therefore, the measurement accuracy will not be good in this small frequency range if an ordinary spectrum analyzer is used.

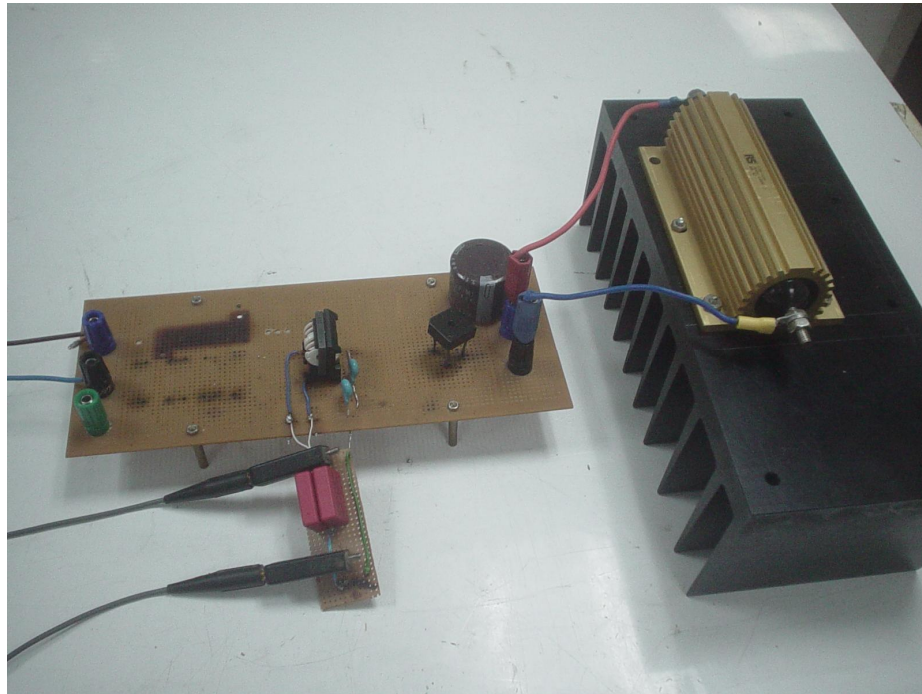


Figure 5.9 Circuit built in lab for the measurement of CM choke's CM impedance

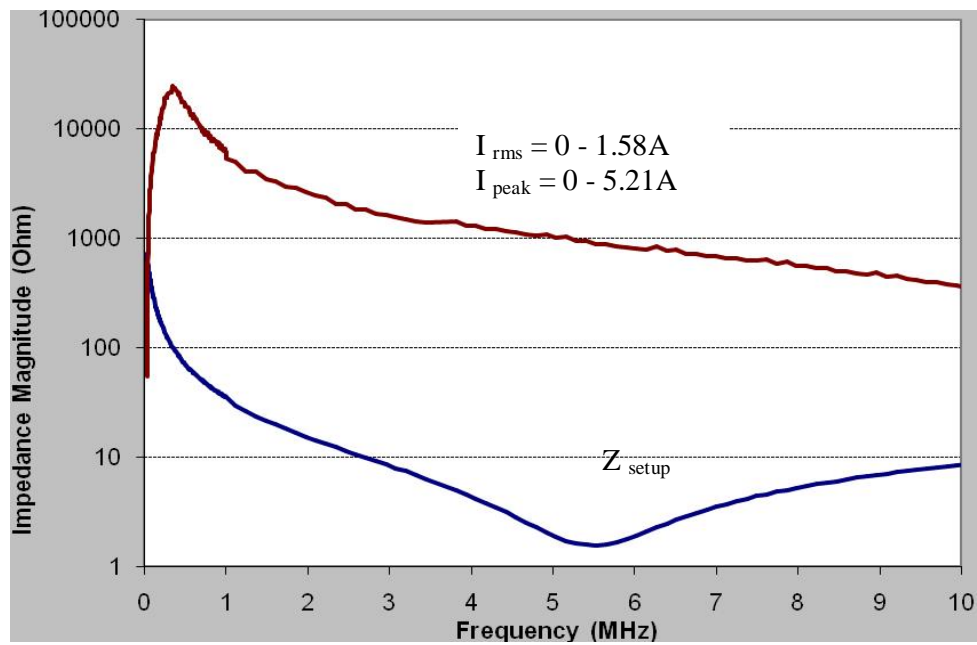


Figure 5.10 The CM impedance and  $Z_{\text{setup}}$

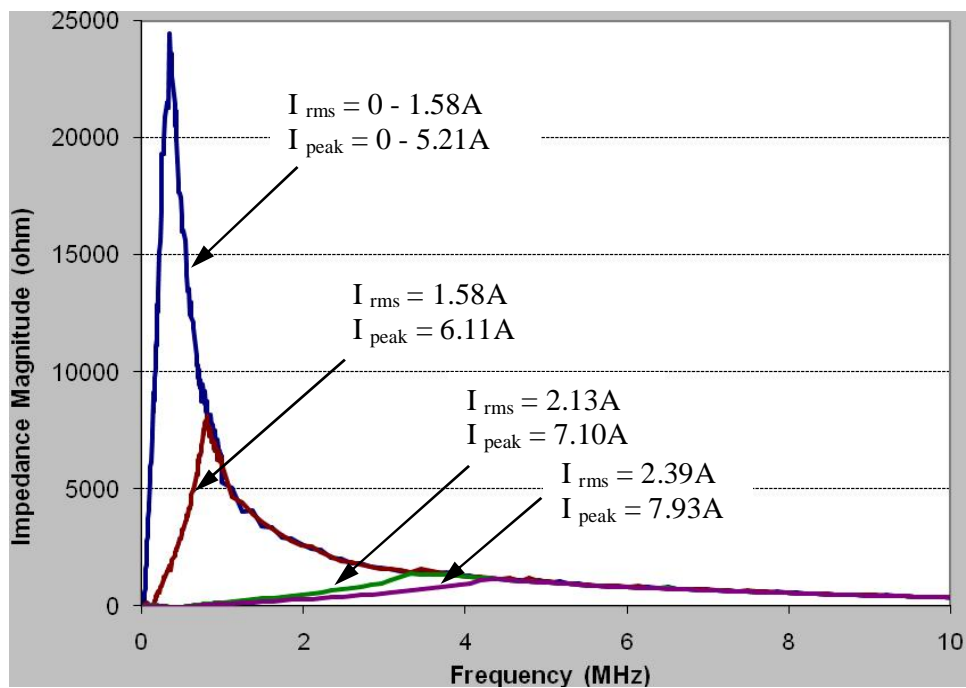


Figure 5.11 The measured CM impedance of the CM choke

Figure 5.12 shows the actual setup for DM impedance measurement of a CM choke. Choke inductors were used to isolate the ac source and load circuit in the measurement. The RF coupling circuit used is identical to that used in the CM impedance measurement. The advantage of fixing the coupling circuit for both setups is that once the calibration is done, the calibration results can be used for both CM and DM setups so that it speeds up the process of CM and DM impedance measurements for CM choke.

The measurement procedures are also identical to that in the CM impedance measurements. The measurement was performed in the frequency range from 50 kHz to 30 MHz at various load currents. Figure 5.13 shows the results of the DM impedance measurement. Ideally, a CM choke should not have exhibited DM attenuation. As explained earlier, the imperfect cancellation of magnetic fluxes in the core due to the two windings of the CM choke results in finite resultant flux in the core, and it leads to finite DM inductance (usually 1 to 3 % of the CM inductance). From the results, it can be clearly observed that when the load current is below 1.83A (rms), the DM impedance of the CM choke exhibits a self-resonate frequency of around 7.1 MHz with magnitude as high as 11 k $\Omega$ . Once the load current exceeds 1.83 A, the magnitude of DM impedance of the CM choke decreases with increasing load current. It is also observed that the drop of CM impedance is more significant as compared to the DM impedance when load current increases, which indicates that the impact of core saturation has a greater impact on CM impedance than DM impedance. This is an interesting finding and will be further investigated as a future research work.



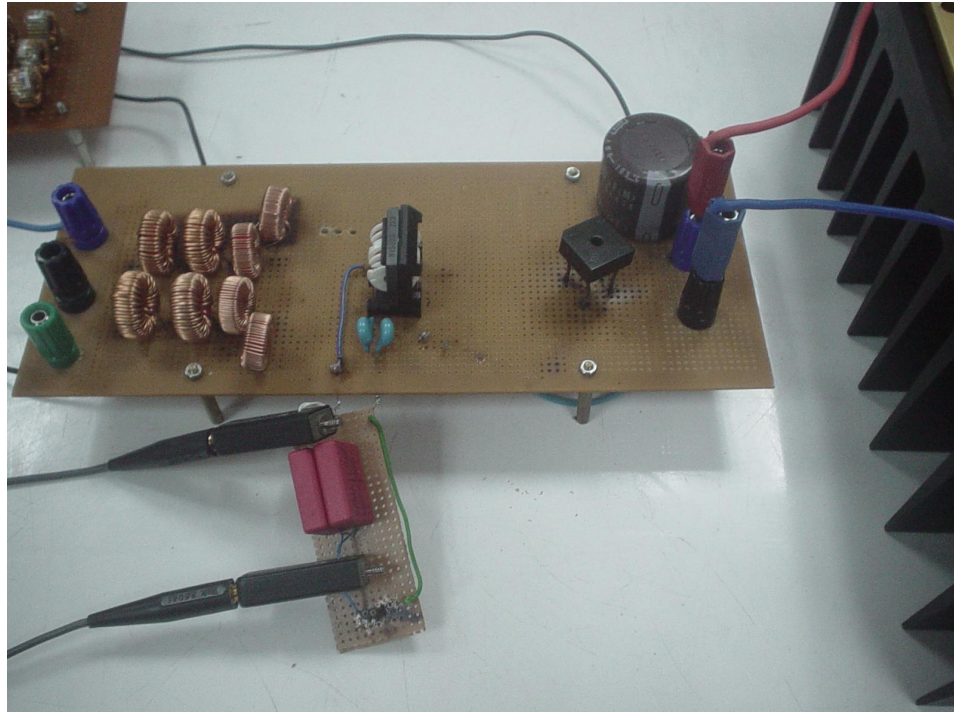


Figure 5.12 Circuit for the measurement of CM choke's DM impedance

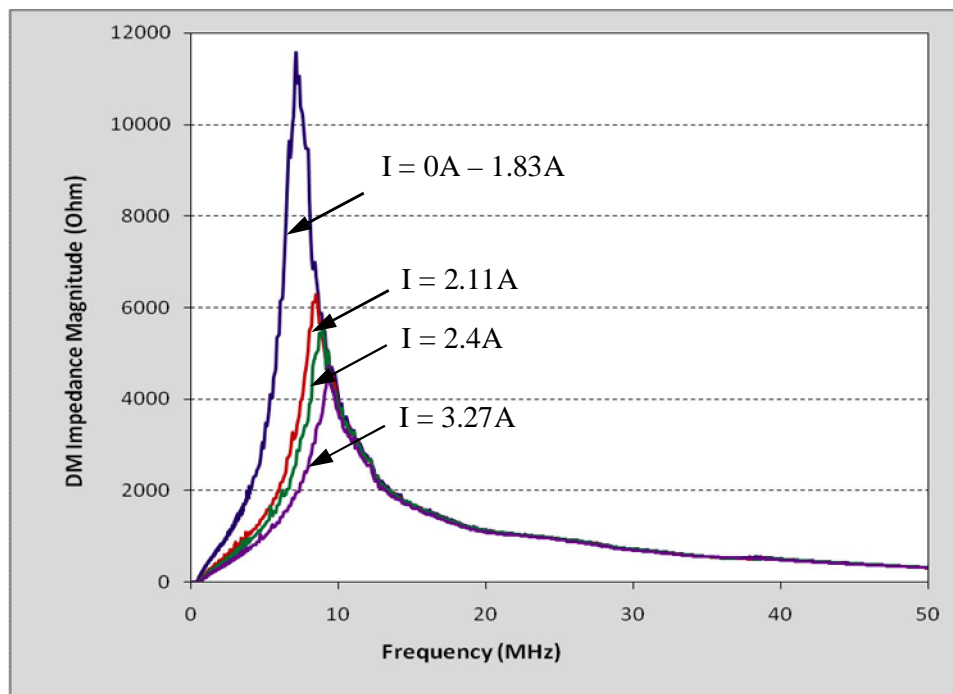


Figure 5.13 The measured DM impedance of the CM choke



## Chapter 6 Conclusions

The theory of the two-current-probe method has been described and its validity has also been experimentally verified. As the two-current-probe setup allows measurement of the noise source impedance of the SMPS under the normal “power on” condition, it has the flexibility to determine the noise source impedance of the SMPS for different loading conditions. The merit of the two-current-probe setup is its pre-measurement calibration process for the RF coupling circuit. With this calibration process, the impedance due to the RF coupling circuit,  $Z_{setup}$ , can be measured and accounted for. Hence, possible error contributed by the RF coupling circuit can be eliminated to achieve good accuracy for the measurement of noise source impedance of the SMPS. For SMPS with high power rating, special attention must be paid to ensure that the CM and DM chokes are not saturated while providing the necessary RF isolation. This can usually be resolved by putting two chokes of lower inductances and higher current ratings in series.

It has also been demonstrated that the two-current-probe measurement approach can be extended to characterize the impedance of CM choke and DM choke under in-circuit condition with its actual operating configuration, which will give us better picture of their performance in the application. Same as in the measurement of noise source impedance of SMPS, the pre-measurement calibration and characterization processes allow the measurement error contributed by the setup to be accounted for

and eliminated, hence, good measurement accuracy can be preserved. The ability to observe the CM choke characteristic under varying load current provides the designer a more complete picture of the EMI suppression performance of the CM choke, without the usual trial-and-error approach.

With the known noise source impedance and the EMI choke impedance under actual in-circuit operating condition, power line EMI filter can be easily designed in a systematic manner.

Some possible applications of the proposed measurement approach can also be extended to the following areas:

1. Characterization of the RF impedance of ac mains input port for various conducted emissions test setups. This will help us to study the impacts of various measurement setups in the measurement results.
2. RF impedance characterization for various ports such as signal ports, telecommunication ports, dc power port, ac power ports, etc. of various electronic equipment and modules.

# References

- [1]. Mitsubiko Kanda and Katsumi Tomiyama, “A Study on Design of EMI Line Noise Filters”, 1997 International Symposium on Electromagnetic Compatibility Proceedings, 1997, pp.527 –530
- [2]. Mark J. Nave, Power Line Filter Design for Switched-Mode Power Supplies, Van Nostrand Reinhold, 1991
- [3]. Laszlo Tihanyi, Electromagnetic Compatibility in Power Electronics, IEEE Press, 1995
- [4]. International Electrotechnical Commission, International Special Committee on Radio Interference, “CISPR 16-1, Specification for radio disturbance and immunity measuring apparatus and methods, Part 1, Radio disturbance and immunity measuring apparatus”, Edition. 2.1, CISPR Publications, Oct. 2002
- [5]. International Electrotechnical Commission, International Special Committee on Radio Interference, “CISPR 16-2, Specification for radio disturbance and immunity measuring apparatus and methods, Part 2, Methods of measurement of radio disturbance and immunity ”, edition 1.2, CISPR Publications, Oct. 2002
- [6]. International Electrotechnical Commission, International Special Committee on Radio Interference, “CISPR 22, Information technology

## Reference

---

- equipment – Radio disturbance characteristics – Limits and methods of measurement ”, fifth edition, CISPR Publications, April 2005.
- [7]. American National Standards Institute “ANSI C63.4-2001 American National Standard for Methods of Measurement of Radio-Noise Emissions from Low-Voltage Electrical and Electronic Equipment in the Range of 9 kHz to 4 GHz”, 2001
- [8]. Mitsuhiko Kanda and Naoto Oka, “A Study of Evaluation Method for Line Noise Filters Using Common Mode Output Impedance of Electrical Equipment”, 1999 International Symposium on Electromagnetic Compatibility, 1999, pp.40 –43
- [9]. Lon M. Schneider, “New Techniques Make Power-Line Emissions Filter Selection Easy”, Interference Technology Engineers’ Master, 1987
- [10]. J. A. Ferreira, P. R. Willcock, and S. R. Holm, “Sources, paths and traps of conducted EMI in switch mode circuits”, Proc. PESC, Vol. 2, pp.1140 – 1145, 1998.
- [11]. American National Standards Institute “ANSI C63.13-1991 American National Standard, Guide on the Application and Evaluation of EMI Power-Line Filters for Commercial Use”, 1991
- [12]. International Electrotechnical Commission, International Special Committee on Radio Interference, “CISPR 17, Methods of measurement of the suppression characteristics of passive radio interference filters and suppression components ”, CISPR Publications, 1981

## *Reference*

---

- [13]. “MIL-STD-220B, Test method standard, method of insertion loss measurement” Department of Defense, USA, 24 January 2000
- [14]. Michel Mardiguian and Joel Raimbourg, “An Alternate, Complementary Method for Characterizing EMI Filters”, 1999 IEEE International Symposium on Electromagnetic Compatibility, Vol.2 1999, pp.882-886
- [15]. Byron Garry and Robert Nelson, “Effect of Impedance and Frequency Variation on Insertion Loss for a Typical Power Line Filter”, 1998 IEEE International Symposium on Electromagnetic Compatibility, Vol.2, 1998, pp.691 -695
- [16]. Schneider L. M. "Noise source equivalent circuit model for off-line converters and its use in input filter design", Proc. IEEE EMC Symposium, 1983, pp. 167-175.
- [17]. D. Zhang, D. Y. Chen, M. J. Nave, and D. Sable, "Measurement of noise source impedance of off-line converters", IEEE Transaction on Power Electronics, Vol. 15, No. 5, Sept 2000, pp. 820-825.
- [18]. International Electrotechnical Commission, "IEC Guide 107, Electromagnetic compatibility – Guide to the drafting of electromagnetic compatibility publications
- [19]. Clayton R. Paul, Introduction to Electromagnetic Compatibility, John Wiley & Sons, 1992, pp.449-487, second edition 2006.
- [20]. J. R. Nicholson and J. A. Malack, “RF impedance of power-lines and line impedance stabilization networks in conducted interference

## Reference

---

- measurements”, IEEE Trans. Electromagnetic Compatibility, vol. EMC-15, no 2, pp. 84-86, May 1973
- [21]. R. A. Southwick and W. C. Dolle, “Line impedance measuring instrumentation utilizing current probe coupling”, IEEE Trans. Electromagnetic Compatibility, vol. EMC-13, no 4, pp. 30-36, Nov. 1973
- [22]. Peter J. Kwasniok, Man D. Bui, A. James Kozlowski and Stanislaw S. Stuchly, “Technique for Measurement of Power line Impedances in the Frequency Range from 500kHz to 500MHz”, IEEE Trans. on Electromagnetic Compatibility, Vol.35, No.1, 1993, pp.87-90
- [23]. A. A. Toppeto, “Test method to differentiate common mode and differential mode noise,” in Proc. IEEE EMC Symp., Rotterdam, Netherlands, 1979, pp. 497-502.
- [24]. Yuang-Shung Lee, Yu Shu, “Line filter design of switching mode power supply using software approximation for conducted emission separation”, The fifth International Conference on Power Electronics and Drive Systems, 2003, PEDS 2003, Volume 2, 17-20 Nov. 2003, pp.1339 – 1344.
- [25]. Yuang-Shung Lee; Yu-Lin Liang; Ming-Wang Cheng; “Time Domain Measurement System for Conducted EMI and CM/DM Noise Signal Separation”, International Conference on Power Electronics and Drive Systems, 2005, PEDS 2005, Volume 2, 28-01 Nov. 2005 pp. 1640 - 1645

## Reference

---

- [26]. Y.-K. Lo, H.-J. Chiu, and T.-H. Song, "A software-based CM and DM measurement system for the conducted EMI," *IEEE Trans. Ind. Electron.*, vol. 47, no. 4, pp. 977–978, Aug. 2000.
- [27]. T. Guo, D. Y. Chen, F. C. Lee "Separation of the Common-Mode and Differential-Mode Conducted EMI Noise", *IEEE Transactions on Power Electronics*, vol. 11, no.3, May, 1996, pp.480-487.
- [28]. Clayton R. Paul and Keith B. Hardin, "Diagnosis and Reduction of Conducted Noise Emissions", *IEEE Trans. on Electromagnetic Compatibility*, Vol.30, No.4, 1988, pp.553-560
- [29]. K. Y. See, "Network for Conducted EMI Diagnosis", *Electronics Letters*, Vol.35 No.17, 19<sup>th</sup> August 1999, pp.1446-1447
- [30]. John C. Fluke, Sr. "Controlling conducted emissions by design", Van Nostrand Reinhold, New York.
- [31]. Wu Xin, M. H. Pong, C. M. Lee and Z. M. Qian, "Reduction of EMI by Electric Field Method", *Applied Power Electronics Conference and Exposition, APEC '99*, Vol.1, 1999, pp.135 –138
- [32]. Mahinda Vilathgamuwa, J Deng, K J Tseng, "EMI suppression with switching frequency modulated dc-dc converters", *IEEE Industry Applications Magazine*, Nov/Dec. 1999, pp. 27-33.
- [33]. Mahinda Vilathgamuwa, Deng Junhong, "Mitigation of conducted EMI in quasi-resonant converters by frequency modulation", *IEEE Industry*

## Reference

---

- Application Society 1996 Annual Meeting, San Diego, USA, Oct. 5-10, 1996.
- [34]. Richard Lee Ozenbaugh, "EMI Filter Design", second version, Maecel Dekker, 2001., TK 7872.F5, Z99, 2001
- [35]. Shou Wang, Fred. C. Lee, Dan. Y. Chen, Willem Gerhardus, "Effects of Parasitic Parameters on EMI Filter Performance", IEEE Transactions on Power Electronics, Vol. 19, No. 3, May 2004.
- [36]. J. A. Malack and J. R. Engstrom, "RF impedance of United States and European powerlines," IEEE Trans. on Electromagnetic Compatibility, vol. EMC-18, no. 1, pp. 36-38, Feb. 1976.
- [37]. R. M. Vines, H. J. Trussel, K. C. Shuey, and J. B. O'Neal, "Impedance of the residential power-distribution circuit," IEEE Trans. on Electromagnetic Compatibility, vol. EMC-27, no. 1, pp. 6-12, Feb. 1985
- [38]. F. D. Martzloff and H. A. Gauper, "Surge and high-frequency propagation in industrial power-lines," IEEE Trans. On Industrial Application, vol. IA-22, pp. 634-640, Jul./Aug. 1986.
- [39]. M. Tanaka, "High frequency noise power spectrum, impedance and transmission loss of power-line in Japan on intrabuilding power-line communications," IEEE Trans. on Consumer Electronics, vol. CE-34, no. 2, pp.321-326, May 1988.



## Reference

---

- [40]. M. M. Forti and L. M. Millanta, "Power line impedance and the origin of the low-frequency oscillatory transients," *IEEE Trans. on Electromagnetic Compatibility*, vol. 32, no. 2, pp. 87-97, May 1990.
- [41]. M. Tanaka, "Transmission characteristics of a power-line used for data communications at high frequencies," *IEEE trans on Consumer Electronics*, vol. CR-35, no. 1, pp. 37-42, Feb 1989
- [42]. K. Y. See, P. L. So, A. Kamarul, and E. Gunawan, "Radio frequency common mode noise propagation model for power line cable," *IEEE Trans. Power Del.*, vol. 20, no. 4, pp. 2443–2449, Oct. 2005.
- [43]. A. Kamarul, K. Y. See, and P. L. So, "Feasibility study of optical isolator in reducing CM conducted emission from PLC modem," in *Proc. 17th Int. Zurich Symp. Electromagn. Compat.*, Feb. 2006, pp. 424–427.
- [44]. K. Y. See, A. Kamarul and P. L. So, "Reduction of CM noise emissions from PLC modem using optically coupled signaling", *IEEE Trans. on Electromagnetic Compatibility*, Nov. 2006, Vol. 48, No. 4, pp. 648-653.
- [45]. F. Y. Shih and D. Chen *et al.*, "A procedure for designing EMI filters for AC line applications," *IEEE Trans. Power Electron.*, vol. 10, Jan. 1996.
- [46]. Henglin Chen, Limin Feng, Wei Chen, Zhaoming Qian "Modeling and Measurement of the Impedance of Common Mode Noise Source of Switching Converters"

## *Reference*

---

- [47]. S. Qu, D. Chen, "Mixed-mode EMI noise and its implications to filter design in offline switching power supplies", *Power Electronics, IEEE Trans. on*, Volume 17, Issue 4, July 2002, pp.502 – 507.
- [48]. James P. Muccioli, Anthony A. Anthony, "Dynamic testing of a dual line filter for common- and differential-mode attenuation using a spectrum analyzer", *ITEM* 2000
- [49]. Mitsuhiko Kanda, Naoto Oka, Shuichi Nitta, "Common Mode Impedance Model of Power Electronic Equipment to Evaluate Noise Reduction Effect of a Line Filter", *2000 IEEE International Symposium on Electromagnetic Compatibility*, 2000, pp.65 -70
- [50]. Henry W. Ott, "Noise Reduction Techniques in Electronic Systems" (second edition), Wiley, 1989
- [51]. Tim Williams and Keith Armstrong, "EMC for System & Installation", Newnes, 2000. TK, 7867.2, W727e.
- [52]. Tim Williams, "EMC for Product Designers", third edition, Newnes, 2001. TK, 7867.2, W727, 2001
- [53]. Kermit O. Phipps, Philip F. Keebler, Bradford R. Connatser, "Improving the way we measure insertion loss", *ITEM* 2002.
- [54]. H. M. Schlicke, *Electromagnetic Compatibility. Applied principles of cost-effective control of electromagnetic interference and hazards*. NY: Marcel Dekker, 1982.

## *Reference*

---

- [55]. Meng Jin, Ma Weiming, Zhang Lei, “Determination of Noise Source and Impedance for Conducted EMI Prediction of Power Converters by Lumped Circuit Models”, 2004 35th Annual IEEE Power Electronics Specialists Conference, pp. 3028 – 3033
- [56]. Weidmann, H; Mcmartin, W.I.. “Two Worst-Case Insertion Loss Test Methods for Passive Power-Line Interference Filters”, IEEE Transaction on EMC, Vol. 10, No. 2, Jan. 1968. (Special Filter Issue).
- [57]. International Electrotechnical Commission “IEC 60950-1 Information Technology Equipment – Safety – Part 1 : General Requirements” second edition, 2005 – 12.
- [58]. International Electrotechnical Commission “IEC 601-1 Medical Electrical Equipment – Part 1: General Requirements for Safety”, second edition, 1988.
- [59]. Annapurna Das, Sisir K Das, “Microwave Engineering” international edition 2001, McGraw-Hill.

## Publications by the Author

- [1]. “Assessment of EMI Chokes under Realistic Loading Conditions”, Junhong Deng, Kye Yak See, 2008 Asia-Pacific Symposium on Electromagnetic Compatibility & 19<sup>th</sup> International Zurich Symposium on Electromagnetic Compatibility, 19 – 22 May 2008, pp. 746 – 749.
- [2]. “In-Circuit Characterization of Common-Mode Chokes”, Junhong Deng, Kye Yak See, IEEE Transaction on Electromagnetic Compatibility, Vol. 49, No. 2, May 2007, pp. 451-454.
- [3]. “Characterization of RF Noise Source Impedance for Switched Mode Power Supply”, Junhong Deng, Kye Yak See, 17<sup>th</sup> International Zurich Symposium on Electromagnetic Compatibility 2006, pp. 537 – 540.
- [4]. “Measurement of Noise Source Impedance of SMPS Using a Two Probes Approach”, Kye Yak See, Junhong Deng, IEEE Transactions on Power Electronics, Vol. 19, No. 3, May 2004, pp. 862-868.